Stober *et al. Swiss Journal of Geosciences* (2025) 118:8
https://doi.org/10.1186/s00015-025-00480-z

SGG SGS sc | nat
Swiss Journal of Geosciences

RESEARCH Open Access

Origin and development of the geothermal fluids of the Baden-Baden area (SW-Germany): implications for geothermal systems of granitic reservoirs

Ingrid Stober[1*], Jens C. Grimmer[2] and Michael Kraml[3]

Abstract

The Baden-Baden thermal springs, among the hottest in Germany, emerge on the south-eastern slope of Florentinerberg, c. 25 m above the Oos valley floor. These Na-Cl-rich waters, with temperatures up to 69 °C, originate from a deep reservoir within the crystalline basement, likely the Nordschwarzwald batholith. New investigations, including hydrochemistry, isotopic data, geothermometry, and structural geological data reveal a deep origin for these waters with reservoir temperatures of c. 176 °C as constrained from various methods. Although the thermal waters (springs, boreholes) emerge from different lithologies (granites, metamorphic schists, Upper Carboniferous rocks), major and trace element concentrations are very similar implying no or only little impact of the different lithologies. The thermal waters are of Holocene age, recharged by meteoric water in c. 900 m asl. Holocene age is backed up by recalculated ^{14}C data yielding a mean residence time of 10,800 years. Hydrochemical and isotopic data indicate interaction with granitic rocks in the subsurface. NE-trending structures in Baden-Baden likely act as hydraulic barriers forcing the thermal waters to the surface. While none of the faults in the thermal spring area is favorably oriented in the stress field it is suggested that the steep SE-plunging intersection of their damage zones facilitate their ascent.

Keywords Thermal water, Hydrochemistry, Isotopes, Geothermometry, Granitic reservoir, Structural geology

1 Introduction

Faults play a crucial role in the migration of fluids within the crust, often acting as the principal conduits for groundwater, hydrocarbons, and hydrothermal fluids (Mitjanas et al., 2024, Faulkner et al., 2010, Agemar et al., 2017, Stober et al., 2016, Bucher et al., 2009a, 2009b; Caine et al., 1996). Large fault zones develop clay-rich, predominant plastically deforming shear zones in their cores, surrounded by predominant brittlely deforming damage zones with enhanced hydraulic conductivity (e.g. Caine et al., 1996; Choi et al., 2016) enabling hot fluids to rise from the depth and form thermal springs at the earth surface unless no sealing rocks inhibit their free outflow. However, prior to drilling into, hydraulic properties of faults are unknown and frequently they exhibit both, high and low permeablities. Topographic differences between mountains and valleys often induce high hydraulic gradients, which are the driving force and precondition of a deep fluid circulation system, recharged by meteoric water infiltrating in the mountains and discharged as thermal springs at the foothills. Highly permeable, steep structures like fault zones are necessary to drain, collect,

Handling editor: Benoit Valley.

*Correspondence:
Ingrid Stober
ingrid.stober@minpet.uni-freiburg.de
[1] Institute of Earth and Environmental Sciences, University of Freiburg, Albertstr. 23B, 79104 Freiburg, Germany
[2] Karlsruher Institut für Technologie (KIT), Institut für Angewandte Geowissenschaften, Adenauerring 20B, 76131 Karlsruhe, Germany
[3] Vulcan Energie Ressourcen GmbH, Amalienbadstr. 41, 76227 Karlsruhe, Germany

and transport thermal waters to the surface, whereas the fault core could act as a hydraulic barrier inhibiting across-fault flow and the damage zone as ascending path for deep thermal waters (e.g. Stober, 1995; Faulkner et al., 2010; Mitjanas et al., 2024).

The up to 69 °C hot thermal springs of Baden-Baden are located close to the Eastern Main Boundary Fault (EMBF) system of the Upper Rhine Graben (URG, Fig. 1) along with other thermal springs, but with lower outflow temperatures of < 40 °C. The Baden-Baden thermal springs emerge on the south-eastern slope of the Florentinerberg from the depth with outflow temperatures between 52.1 and 69 °C. These springs are renowned as the hottest, most enriched in dissolved solids in Baden-Württemberg with sodium and chloride as the main components.

The free outflowing thermal springs are known since ancient times, at least since the early third century, documented by relic Roman ruins, or even since Keltic times. In historical times, the original spring in the basement of the Old Steam Bath was the most important and most productive main spring in the thermal district, with a flow rate of 113 m^3 d^{-1}. The thermal water was used for bathing and drinking cures. From the sixteenth century until a few years ago, the hot water was also used for well cures with therapeutic benefits (e.g. Sanner, 2000; Maus & Sauer, 1972; Sauer, 1966). Since the 1870ies, the thermal springs are tapped by subhorizontal artificial galleries (Friedrichstollen, Kirchstollen) driven into Upper Carboniferous sedimentary rocks to collect the thermal water for utilization in the spa areas. The total flow rate of all thermal springs exceeds 800 m^3 d^{-1}. In the 1960ies two 302 m and 553 m deep wells (Florentinerquelle I, II), north of the thermal spring galleries, were drilled to increase the production rate. The two wells tapped the same water type as found in the thermal springs (Maus & Sauer, 1972).

First systematic geological investigations in the area of the thermal springs were carried out at an early stage, as well as initial considerations on the origin and genesis of the highly mineralized hot waters (e.g. Eisele, 1907; Bilharz, 1934; Kiderlen, 1953; Sittig, 1965; Carlé, 1975). However, the high salinity of the waters has often been associated with halite-bearing layers in the URG (Kiderlen, 1953; Sauer, 1966; Carlé, 1975; Metz, 1977). In the years that followed detailed geological

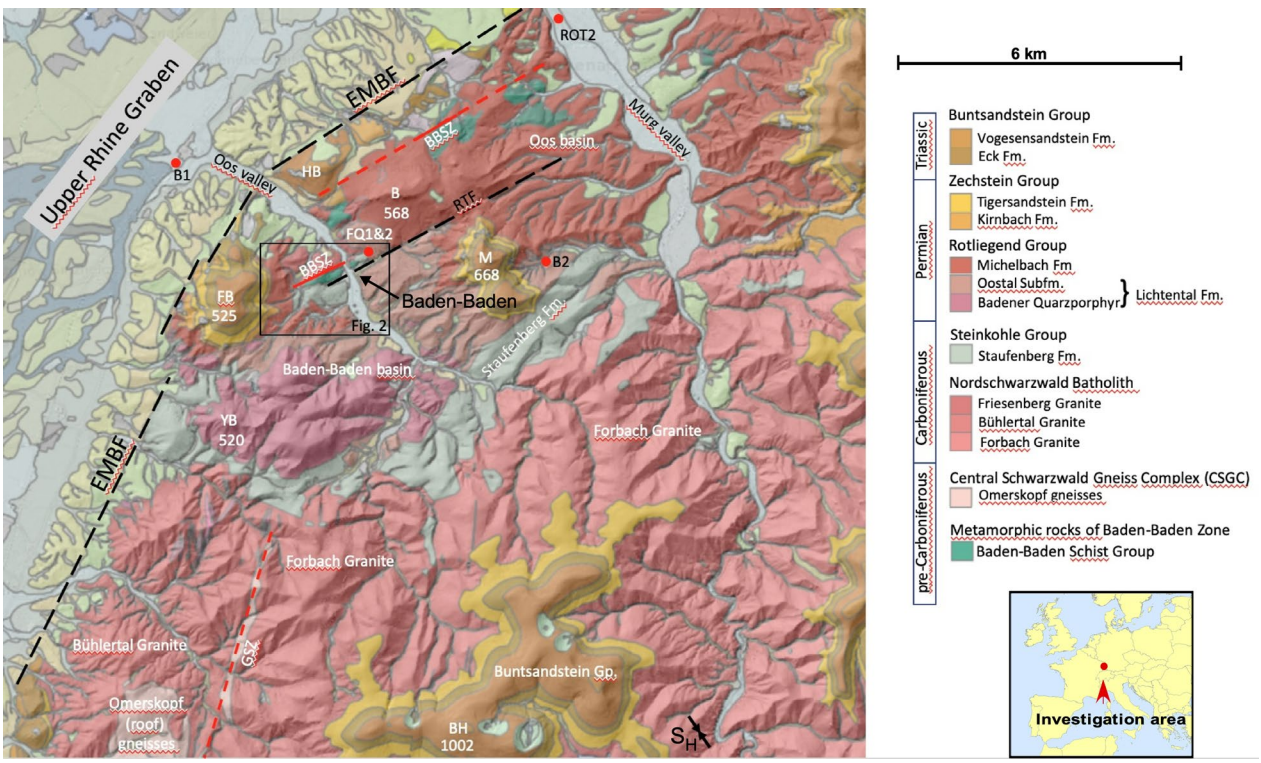

Fig. 1 Geological overview of the investigation area modified from the map viewer of the LGRB (https://maps.lgrb-bw.de). The inset map (lower right) shows the location of the investigation area in Europe, SW-Germany. Mountains are highlighted with numbers referring to their altitudes in meter above sea level (BH: Badener Höhe, M: Merkur, FB: Fremersberg, B: Battert, HB: Hardberg). Boreholes: B1: Baden-Baden 1; B2: Baden-Baden 2 (Staufenberg); FQ1&2: Florentinerquelle I, II; ROT2: Gaggenau-Rotenfels 2. GSZ: Glashütte shear zone; BBSZ: Baden-Baden shear zone; EMBF: Eastern Main Boundary Fault; RTF: Rotenbach fault. The black arrows indicate trend of maximum horizontal stress axis (S_H). See also Fig. 6c

investigations in the Baden-Baden area were carried out by Sittig (1965), Löffler (1988,), Fröhler and Lebede (1987), Zuther and Brockamp (1988), Wickert et al. (1990), Montenari and Servais (2000), and Eisbacher and Fielitz (2010). Between 1980 and 1989 a tunnel was built on the western side of the Oos valley to relieve traffic volume in the city center. Within the tunnel slightly elevated temperatures and water with elevated concentrations (TDS) were observed (Müller-Hereth, 1982; Fröhler & Lebede, 1987; Basler, 1989b). Additionally, from the late 1960s to 1990s major investigations (boreholes, trenches) for underground constructions (parking garages, tunnel) in the city area provided new geological data, which are considered in the official geological map (https://maps.lgrb-bw.de).

First modern hydrogeological investigations concerning origin and development of the main water components were carried out by Stober (1995, 1996) and Stober and Bucher (1999a, 2004), deducing the main water components as well as the high salinity by a deep circulation system and by chemical interaction of meteoric surface water with the granitic reservoir rock and H_2O-consuming alteration reactions. Based on this hydraulic model concept of the deep circulation, Schrage (2004) and Giersch (2006) built a three-dimensional, numerical flow and heat transport model for the assumed catchment area of the thermal springs of Baden-Baden using the simulation software FEFLOW® 5.1 (Giersch, 2006). The resulting model demonstrated the plausibility of the former perception on the genesis of thermal waters from a mathematical and physical point of view and supported the hypothesis that the fluids of the Baden-Baden springs are of meteoric origin, recharged from precipitation in the area of the widely exposed Nordschwarzwald batholith south and southeast of Baden-Baden (Fig. 1) and that they are part of a convection cell which reaches as deep as 3500 m below sea level in the fractured basement. The average residence time of the thermal water thereby is approximately 11,000 years.

In the Baden-Baden area thermal fluids are not limited to the thermal spring galleries, occur at various locations, and emerge from different geological units.

In this study we present new data and used new isotopic and hydrochemical investigation methods, including geothermometry, and structural geological data as well as (unpublished) archival and published data including borehole data and drilling reports, also from the nearby Michaels-tunnel, to provide a more comprehensive view on origin and development of the thermal fluids in the Baden-Baden area and their geological boundary conditions.

For geothermal systems in use, central questions regarding the origin of the fluid, the quantitative fluid genesis and the spatial–temporal dimensions of a potential regional recharge-discharge system are generally unknown. A quantitative understanding of available fluid volumes, fluid development as well as circulation, transport and storage of fluids in geothermal reservoirs is essential for a sustainable and responsible use of energy and raw materials from deep geothermal fluids, like lithium. In particular, there is generally no quantitative idea of the relative magnitude of the impact on the fluid balance caused by the operation of a geothermal plant. Important parameters (e.g. mean residence times of the fluids in the reservoir) for characterizing these material flows are also lacking, but are necessary for the expansion of utilizing deep geothermal energy. In this work, very different investigation methods are applied and tested on the thermal water springs (and thermal wells) of Baden-Baden, based on a deep circulation system in granitic rocks. We hope that this will provide an impetus and help to carry out comparable investigations in utilized geothermal systems in order to close knowledge gaps regarding the quantification of the genesis, transport and development of the fluids.

2 Geology and tectonic situation of the study area

The thermal springs of Baden-Baden are located on the eastern flank of the NW trending Oos valley c. 20–30 m above the valley floor of the Oos river, which has incised into NE-trending basement and Permocarboniferous cover rocks of the Oos basin (Fig. 1; Sauer, 1966; Stober, 1995, 1996; Rupf & Nitsch, 2008; Eisbacher & Fielitz, 2010). This basin is cut to W by the Cenozoic Eastern Main Boundary Fault system of the URG (EMBF; Fig. 1), plunging beneath Triassic cover to the NE and major WNW trending fault, and bounded to the S and SE by the crystalline basement rocks of the Nordschwarzwald batholith and the Central Schwarzwald Gneiss Complex (CSGC, Fig. 1). Nitsch and Zedler (2009) discriminate the southeastern part of the NE-trending Battert swell as Baden-Baden basin as it is floored by > 200 m of Upper Carboniferous and early Permian volcanic rocks, which are lacking in the Oos basin. There, Permian redbeds were deposited on magmatic and metamorphic rocks (Fig. 1). These Permian redbeds constitute a major NW-directed composite alluvial fan (Löffler, 1988). The generally N-S trending Michaels-Tunnel intersects, from N to S, SE-plunging basement and cover of the Baden-Baden basin (Figs. 1, 2, 3) (Wickert et al., 1990). The crystalline basement was affected by NE-striking mylonitic zones as documented in the Michaels-Tunnel and in natural exposures NNE of it making up the Baden-Baden shear zone (BBSZ, Fig. 1; Krohe & Eisbacher et al.,

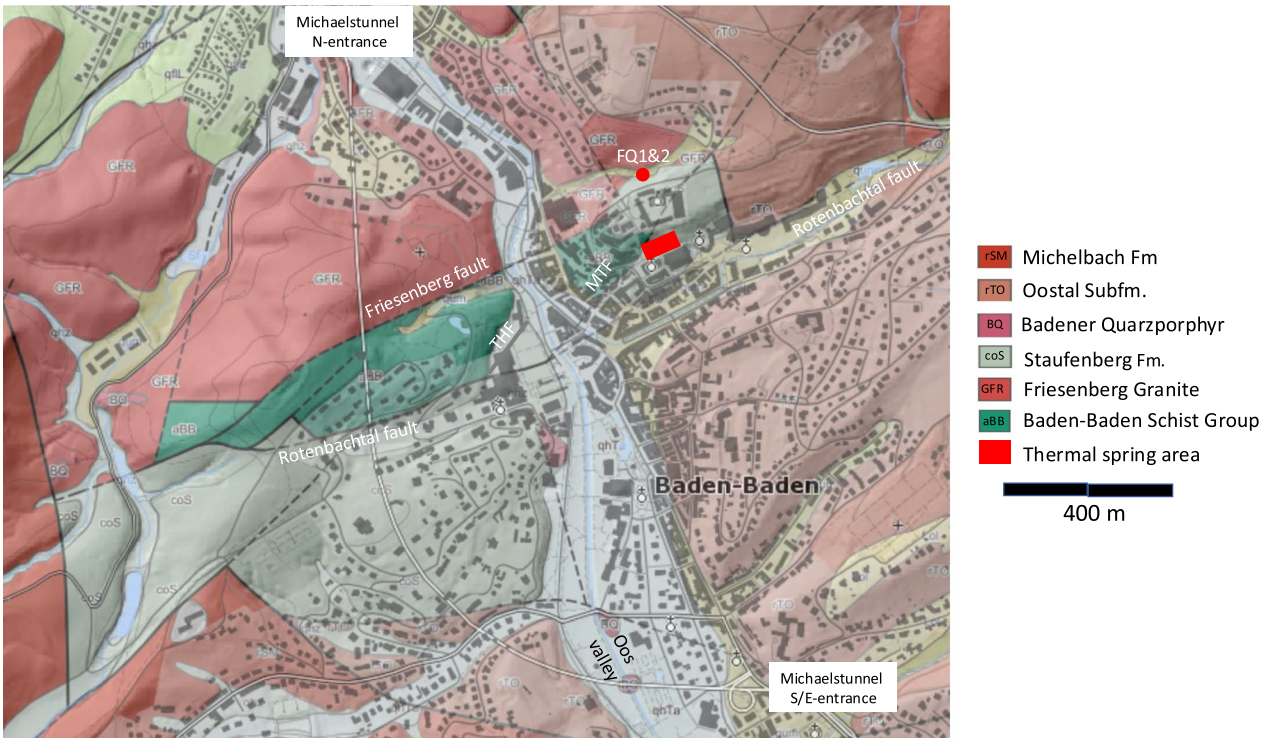

Fig. 2 Simplified geological map of the Baden-Baden city area (location shown in Fig. 1) displaying projected tunnel axis, thermal spring area (red rectangle, for details see Fig. 8), Florentinerquelle boreholes (FQ1&2), main faults discussed in the text, and geological units. *MTF* Main thermal fault, *THF* Trinkhallen fault. Map modified from LGRB-map viewer (https://maps.lgrb-bw.de)

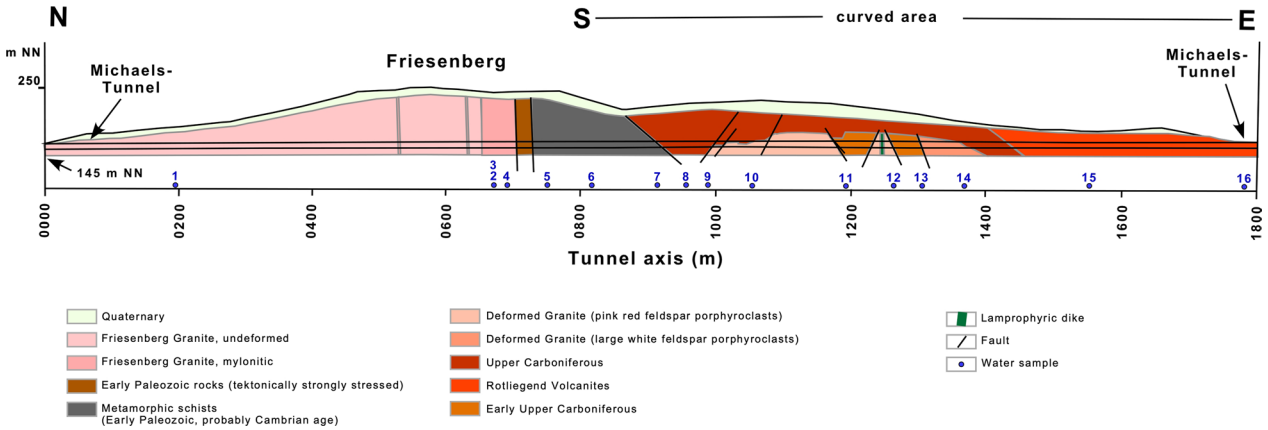

Fig. 3 Geological section along the axis of the Michaels-Tunnel (Löffler, 1988, after report of the tunnel engineering firm Müller-Hereth, 1982). Geology of the tunnel section was reinterpreted using the official geological map of Baden-Baden (https://maps.lgrb-bw.de/) and Fröhler and Lebede (1987). Numbers refer to the collected water samples and their location in the tunnel (Table 1 ESM)

1988; Wickert et al., 1990). The BBSZ possibly offset the NNE-striking Glashütte Shear Zone (GSZ; Fig. 1), a segment of the East Rhine Detachment (Grimmer et al., 2017). Another mylonitic shear zone characterizes the boundary of two mica granites and the Baden-Baden Schist Group (Wickert et al., 1990). Mylonitic shear zones postdate late Early Carboniferous (Visé) granite emplacement and predate late Carboniferous basin formation. This implies exhumation from ductile middle to brittle upper crustal levels during late Carboniferous times. Hence, brittle faulting overprinted the crystalline basement rocks since late Carboniferous times.

2.1 The Battert swell

The 'Battert swell' is bounded to the SE by the Rotenbachtal fault (Eisbacher & Fielitz, 2010) and to the NW by the Friesenberg fault. NW of the Friesenberg fault, NW-dipping normal faults may be regarded as part of the EMBF system (Fig. 1). The Friesenberg fault is a NW dipping reverse fault with the Friesenberg granite in the hanging wall and the Baden-Baden Schist Group in the footwall, separated by a few meter of cataclastic rocks (Figs. 1, 2) (Maus & Sauer, 1972). The 'Battert swell' is cut obliquely by NE- to NNE-striking, (E)SE-dipping faults ('Main thermal fault' and 'Trinkhallen fault') with generally eastward dipping conglomerates, arkosic sandstones, siltstones, minor coal seams of the Staufenberg Formation in the hanging wall and Baden-Baden Schist Group in the footwall (Fig. 2). The thermal spring area is located in the hanging wall of the ´Main thermal fault´, hosted by sedimentary rocks of the Staufenberg Formation. The 'Main thermal fault' and the 'Trinkhallen fault' appear to be cut by the steeply SE dipping Rotenbachtal fault exhibiting in the hanging wall alluvial fan deposits including volcaniclastic (Oos Valley Subformation) and siliciclastic rocks (Michelbach Formation). For further stratigraphic details see Geyer et al. (2011) and Nitsch and Zedler (2009).

2.2 The Michaels-Tunnel section

In the Michaels-Tunnel the contact between the Friesenberg granite and the Baden-Baden Schist Group was mapped as a subvertical ductile shear zone (Wickert et al., 1990; Löffler, 1988; Basler, 1989a, 1989b). The contact between Friesenberg granite and the Baden-Baden Schist Group appears to be of tectonic origin, not only because of identified shear zones and faults, but also because of the absence of contact metamorphic mineral assemblages (Sittig, 1965, Maus & Sauer, 1972).

The c. 1.8 km long Michaels-Tunnel intersected from the northern entrance to the southern entrance SE plunging crystalline basement and cover rocks (Figs. 2, 3): i.e. in the N the Friesenberg granite, the NE-striking Baden-Baden shear zone defining here the contact to the metamorphic rocks. These rocks are in structural contact with the Staufenberg Formation by a several meter thick, NNE striking, cataclastic shear zone (Fig. 3). This shear zone may be regarded as a third NNE-striking ('Michaels-Tunnel') fault segment in addition to the Trinkhallen and Main thermal faults (Fig. 3). At about tunnel meter 900 (TM 900; i.e. 900 m from the northern entrance) the tunnel axis increasingly bends from a north–south to an easterly direction (Fig. 2). At about TM 1000 the tunnel intersects late Carboniferous sedimentary rocks and mylonitic-cataclastic granites, interpreted as E-W-striking horst-graben structures (Fig. 3) (Thuro 1998; Bozorg-Mehri 1989; Löffler 1988). From TM 1400 to the southern tunnel termination the Staufenberg Fm. is overlain by minor intercalated volcanic and volcaniclastic rocks of the Lichtental Fm. and Permian red beds of the Michelbach Fm.

3 Material and methods

3.1 Fluid data and sampling

Published hydrochemical and isotopic data from the thermal springs and the two thermal wells supplying the spa of Baden-Baden and hydrochemical data of water ingressing the Michaels-Tunnel were collected (Sauer, 1966; Carlé, 1975; Stober, 1995; Bender, 1995; Stober & Bucher, 1999b; Bucher & Stober, 2000; Käß & Käß, 2008; Göb et al., 2013; Sanjuan et al., 2016; Basler, 1989b). Thus, time series of water compositions are available for the springs and the two boreholes, where in some cases analytical data date back to the nineteenth century. All hydrochemistry data were checked for plausibility and completeness by comparison with the measured electrical conductivity and by the calculated electrical neutrality of the ion balance.

Additionally, in March 2022 we collected fluid samples from the thermal springs within the two galleries of Baden-Baden for hydrochemical and isotopic analyses. Temperature, electric conductivity (EC), and pH were determined in the field, i.e. on site.

Water samples were collected in new polyethene (PE) bottles. Before collecting water samples, all materials were well flushed with the water to be sampled later. Samples for the cation analytics were filtered with a 0.45-µm membrane filter. To prevent the formation of metal hydroxide complexes, samples for the cations including trace elements were acidified with sub-boiled nitric acid (HNO_3) to pH < 2 immediately after sampling. Samples for anion analytics (SO_4, F, Cl) were stored dark. All samples were kept cool until the day of analysis.

Isotope sampling method: The samples for determination of sulfur and oxygen isotopes of the dissolved sulfate ($\delta^{34}S_{SO4}$; $\delta^{18}O_{SO4}$) 2L-PE-bottles were used and filled up to the rim. The samples were kept dark prior to the analysis.

3.2 Fluid analyses

Major cations were analyzed with an ICP-OES iCAP 7000 radial and a dilution factor of 5 and 10 whereas the trace elements via ICP-MS iCAP RQ (Thermo Fisher) with a dilution factor of 5. As Certified Reference Material (HPS) 'Trace Metals in Drinking Water' (CRM-TMDW) of company High Purity Standards was used. Anions were analyzed undiluted with a Methrom Compact IC 930 using Certified Reference Material 'River Water – Anions' (CRM-LGC6020). Alkalinity had to be

determined via calculation using the ion balance because the titration equipment was missing in the field.

Isotope analyses: Sulfate precipitation of the 25% HCl-acidized (pH < 2) and heated samples was triggered with admixed 8.5% $BaCl_2$ solution. The precipitated $BaSO_4$ was filtered and dried at 40 °C. The sulfur and oxygen isotopes of the dissolved sulfate in the water samples were measured with a ThermoScientific Delta V Advantage gas isotope mass spectrometer. International standards IAEA-S-1, IAEA-S-2, IAEA-S-3, IAEA-SO-5, IAEA-SO-6, and NBS 127 have been used as Certified Reference Materials and Ag2S Lab and BaSO4 Lab as additional internal standards.

3.3 Tunnel and thermal spring gallery geologic data

We collected structural data from the thermal spring galleries, reviewed tunnel reports, with respect to geological and structural data, and analyzed geological maps from the Geological Survey of the Federal State of Baden-Württemberg (LGRB) to identify brittle structures. These structural data are crucial for better understanding fluid flow in crystalline basement rocks of the upper crust.

3.4 Stress data

Data to constrain the regional stress field in the Schwarzwald are derived from few hundred meters deep boreholes and focal plane solutions (von Gehlen et al., 1986; Plenefisch & Bonjer, 1997; Hauser-Fuhlberg et al., 2012; Heidbach et al., 2016; Meixner et al., 2018).

3.5 Borehole data

Temperature- und flowmeter-Logs of the 1960s, carried out in the thermal boreholes Florentinerquelle I and II, were newly evaluated to determine inflow (or outflow) zones into (or out) of the boreholes. The Logs were measured in uncased boreholes.

3.6 Thermodynamic based computations

The code PHREEQC and the LLNL database (Parkhurst & Appelo, 1999) was used to compute distribution of species, species activity, mass transfers and the saturation state with respect to selected minerals of the fluids. The code SUPCRT (Johnson et al., 1992) was used to calculate equilibration reactions between selected minerals and fluids.

4 Results

4.1 Structural geological data

4.1.1 Structural data of thermal spring galleries

The thermal spring galleries intersect grey arkosic sandstones and siltstones of the Upper Carboniferous Staufenberg Formation (Fm). The partial expansion limited a systematic data acquisition along the entire length of the gallery system. Sedimentary strata dip to the NE, E, and SE with moderate to shallow angles (Fig. 4a). Five minor faults within these successions were documented (Fig. 4b) showing ENE trending faults (i.e. striking subparallel to the Rotenbach fault) indicating that the Rotenbach faulting activity postdates deposition of the Staufenberg Fm.

4.1.2 Structural data from the Michaels-Tunnel

4.1.2.1 Upper Carboniferous structures Upper Carboniferous rock overlie metamorphic schists structurally in the hanging wall of a SE dipping, thick cataclastic fault zone (Fig. 4c, d, e). Dip direction of strata is variable, particularly in the fault zone, but generally is to the SE. Dip direction of this fault zone is similar to the Trinkhallen and Main Thermal fault and thus may be regarded as a third NE- to NNE trending fault segment ('Michaels-Tunnel fault') with metamorphic schists in the footwall and Carboniferous sediments in the hanging wall.

4.1.2.2 Structures in the crystalline basement Orientation distribution of joints in both crystalline basement and late Carboniferous to early Permian sediments are varied, but with clear predominant orientations of NNW-SSE (140°–155°), NE-SW (055°–065°), and WSW-ENE (070°–085°) (Fig. 4i). However, it needs to be taken into account that the NNW-striking joints are possibly a bit overrated based

(See figure on next page.)

Fig. 4 Stereographic projections (lower hemisphere, equal area) of bedding (**a**) and faults (**b**) in the thermal spring galleries and bedding (**c**), faults (**d**), and cataclastic shear zones (**e**) in the Michaels-Tunnel (data compiled from Basler, 1989a), both in Upper Carboniferous sediments of the Staufenberg Fm., orientation of brittle faults in crystalline basement rocks in the Friesenberg granite (**f**), in metamorphic schists (**g**), and in mylonitic cataclastic two-mica granites (**h**), Rose diagram (**i**) showing statistic distribution of joints dipping steeper than 50° in crystalline basement and late Carboniferous to early Permian sediments (data from the first 1.5 km of the Michaels-Tunne; compiled from Basler, 1989a), and Stereographic plot (**j**) of stress axes orientation obtained from overcoring triaxial cell data of granites in boreholes of the eastern Murg valley flank (Fig. 1; data compiled from Hauser-Fuhlberg et al., 2012; bold symbols represent mean values of individual measurements)

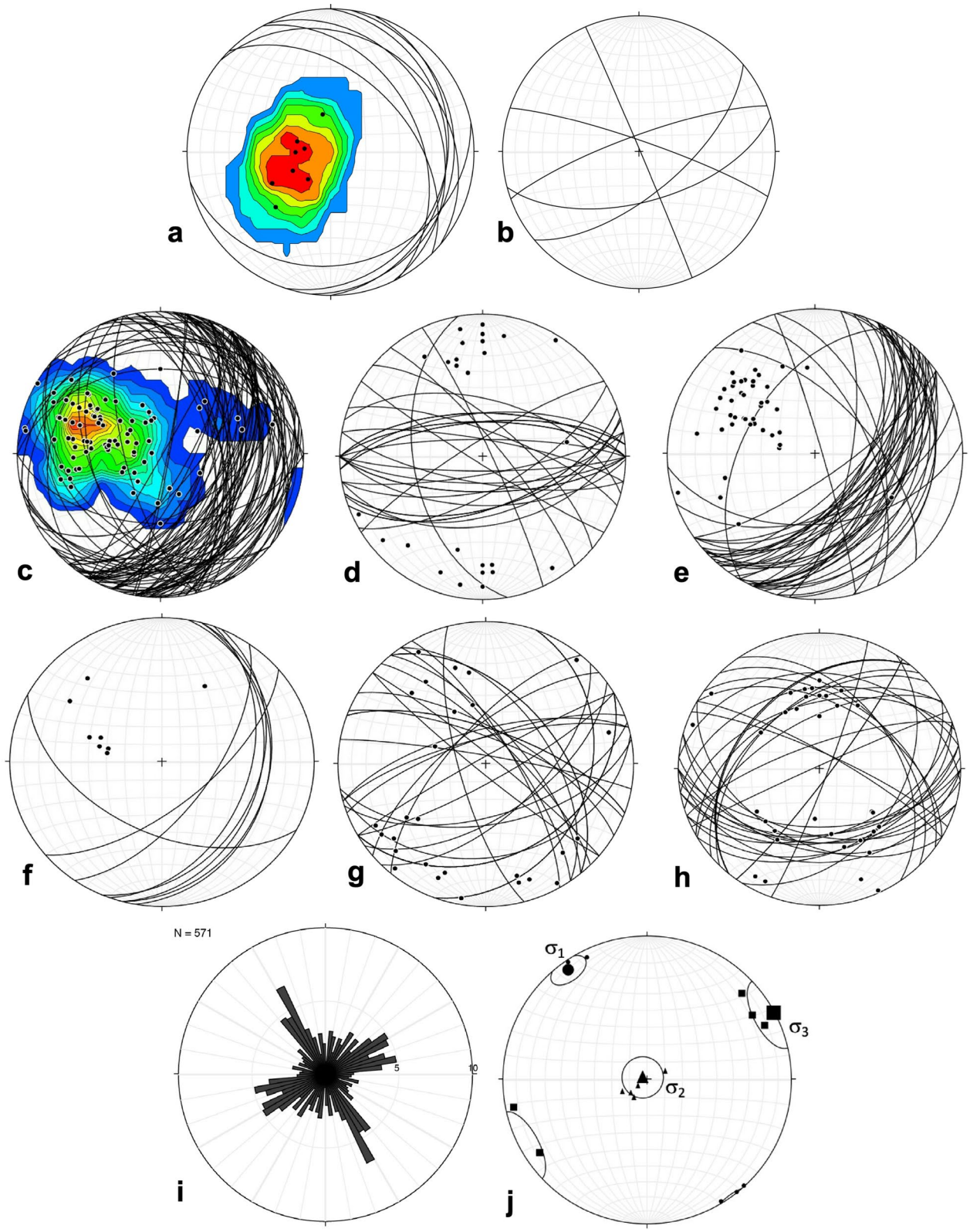

Fig. 4 (See legend on previous page.)

on multiple documentation during tunnel construction progress N-S- to NW-SE-trending sections of the tunnel. Figure 4f, g, h show the orientation data of brittle faults of the Friesenberg granite, the metamorphic schists, and the mylonitic-cataclastic granites. For the Friesenberg granite faults dip to ESE to SE with one fault dipping to the SW while no NW dipping fault was documented. In the metamorphic schists brittle faulting patterns are much more varied: predominant directions are NW- and NE-striking faults. For the mylonitic-cataclastic granites brittle faults predominantly strike E-W, NW-SE, and NE-SW. A minor suite of faults strikes NNE. The proposed E-W-striking horst-graben structure between TM 1000 and TM 1400 is not reflected by brittle fault data (Fig. 4f, g, h) and these alternating basement-cover tectonic blocks thus rather strike NE-SW than E-W.

4.1.3 Stress data

The maximum horizontal stress axes (S_{Hmax}) trend relatively uniform (N)NW-(S)SE in the Schwarzwald (von Gehlen et al., 1986; Heidbach et al. 2016). In the Murg valley, c. 15 km SE of Baden-Baden, stress data from overcoring triaxial cells in boreholes in granite (Hauser-Fuhlberg et al., 2012) indicate for the orientation of 325/01 for S_H (σ_1), 061/05 for S_h (σ_3), and a subvertical orientation for S_V (σ_2). Stress gradients, based on three data points, for S_h are calculated to 17.5 MPa/km, to 27.1 MPa/km for S_V, and to 46.9 MPa/km for S_H, compatible with a strike-slip regime (Fig. 4j). In spite of the methodological uncertainties (overcoring, shallow boreholes, few data, topography effects) the results appear regionally consistent and geologically reasonable.

4.2 Hydrochemistry of waters in the Michaels-Tunnel

During construction of the Michaels-Tunnel fluids discharging into the tunnel were sampled and analyzed with regard to construction materials for the tunnel and in order to identify possible thermal spring waters. This monitoring was needed to be prepared for initiating mitigation measures in case thermal water outflow into the tunnel and a pressure drop in the thermal spring galleries was unintendedly generated by tunnel construction. Analyses of the tunnel water samples (in mg kg^{-1}; laboratory Dr. Stavenov) are presented in the Electronical Supplementary Materials (ESM).

Maximum overburden of the Michaels-Tunnel is ca. 100 m (Fig. 3). Despite the low overburden, TDS of the collected water samples in the tunnel varies between 223.0 and 3186.5 mg kg^{-1} (Table 1 ESM). Slightly enhanced water temperatures (≥ 15 °C) are documented along the entire section between sample no. 2 and 9. The highest temperature in tunnel water samples were observed in the samples no. 6 and 7 with 17.3 °C, resp. 17.2 °C (Table 1 ESM). Tunnel ventilation with low air temperature and the very low discharge rates (few mL s^{-1}) of the collected waters in the tunnel generally compromise temperature measurements towards lower values. Water sample no. 7 was taken from a c. 20–50 cm thick zone, which was nearly dry (Fig. 3).

Figure 5A shows the main components of the water, sampled in the Michaels-Tunnel, in a Schoeller-Diagram. Additionally, for comparison reasons, the water composition of the Florentinerquelle II as a proxy for the thermal spring waters of Baden-Baden is included. Some of the tunnel waters, especially no. 8, 9, and 10, collected in Upper Carboniferous sediments (no. 8) and mylonitic-cataclastic granites (no. 9, 10), are with respect to the water type very similar to the thermal spring water, but differ in lower TDS. So, they seem to be diluted by meteoric water. Tunnel water samples no. 6 and 7, collected in the metamorphic schists have as well quite high sodium and chloride concentrations, resembling the thermal spring water, but differ in higher HCO_3 contents. These samples outline the highest TDS of all tunnel-waters. Sample no. 11, collected in the (early) Upper Carboniferous sediments (Fig. 3), is as well strongly influenced by thermal spring water. In nearly all tunnel waters, except for samples no. 3 and 4, chloride concentration is enhanced (Table 1 ESM). However, samples no. 1 and 16 might be influenced by road salting. Highest Cl values are documented in samples no. 6–10 with concentrations > 1000 mg kg^{-1}.

The highest impact of thermal spring water along the tunnel section occurs in water samples no. 6–10, i.e. SE of the 'Battert horst' in the metamorphic schists, in the Upper Carboniferous sedimentary rocks, and in the mylonitic-cataclastic granites. The samples no. 8, 9, and 10 best fit to the thermal spring water. Thus, waters from different lithological units, particularly in the central part of the tunnel, display a certain, slightly variable component of the typical thermal spring water of Baden-Baden, likely admixed to minor degrees with shallow groundwater.

4.3 Hydrochemistry of the Baden-Baden thermal waters

4.3.1 Location of the thermal waters

The spa Baden-Baden receives its thermal water from thermal springs and from thermal wells.

4.3.1.1 Thermal spring galleries The thermal springs are located on the south-eastern slope of the Florentinerberg, about 20–30 m above the bottom of the Oos valley floor (red rectangle in Fig. 2). In historic times the thermal springs were flowing out freely and built up a travertine fan at the foothill of the Florentinerberg. When the spa district was redesigned and the Friedrichsbad was

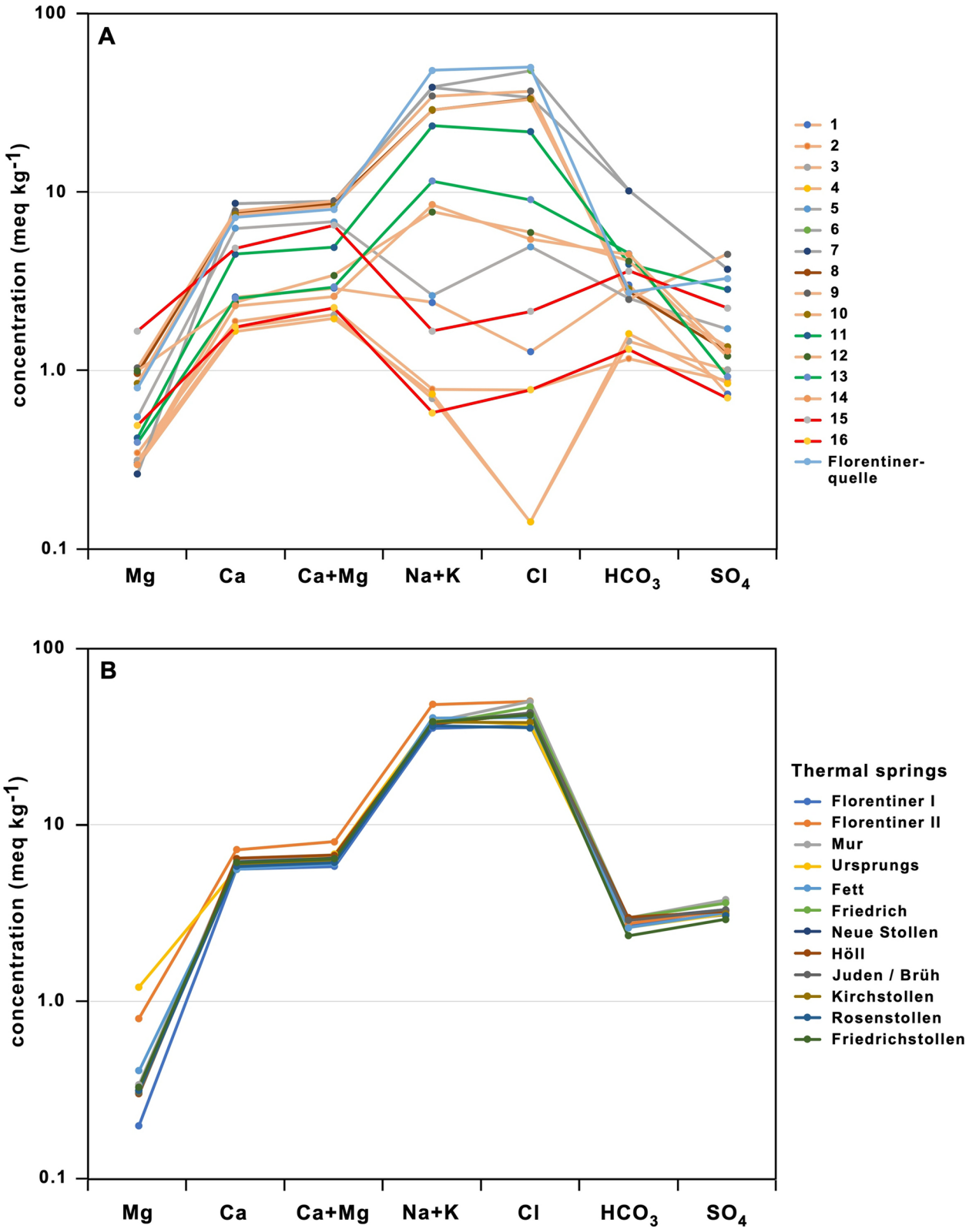

Fig. 5 Schoeller-diagrams: **A** water samples of the Michaels-Tunnel (Table 1 ESM); numbers refer to the sampling locations in the tunnel (Fig. 3), **B** thermal waters of Baden-Baden (Table 2 ESM)

rebuilt in 1868–1871, two branched tunnel systems were constructed into the strata of the Upper Carboniferous to collect the most important thermal water outlets, to increase the flow rate and to protect the springs from bacteriological contamination. During excavation of the Friedrichstollen the thermal springs Brüh-, Juden-, and Ungemachquelle (Fig. 6) dried up temporarily, but were later channeled together. After extensions were made at the turn of the nineteenth and twentieth century, the total length of these galleries today is around 200 m.

Within the galleries, the thermal water emerges in several springs with temperatures of up to 69 °C along faults, fractures and fissures in the Upper Carboniferous in the hanging wall of the Main thermal-fault, i.e. SE of it (Fig. 6). The Upper Carboniferous sediments in the galleries consist of alternating layers of arkosic sandstones, fine-grained sandstones, conglomerates, shales, and minor thin coal seams. According to Bilharz (1934) it is tectonically strongly stressed and dominated by small normal faults, inclined in SE direction. According to the geological section along the Michaels-Tunnel (Fig. 3) and exposures of the galleries, the thickness of the Upper Carboniferous is expected to be low (< 100 m) and overly granites.

The so-called Main thermal fault, a normal fault zone, separates the metamorphic schists from the Upper Carboniferous rocks in the thermal spring gallery area. This fault-zone runs from SW to NE passing NW of the galleries, i.e. all thermal springs are situated SE of the Main thermal fault and the fault runs outside the galleries, i.e. it is not exposed in the galleries. The Main thermal fault is cut by the Friesenberg reverse fault towards N. In SW direction the Main thermal fault is cut by the Rotenbach fault, which strikes subparallel with the Friesenberg fault (Fig. 158 in Metz, 1977) (Fig. 2). From constructional projects in the Oos valley and the city center, which intersected and removed parts of the Quaternary cover, it is known that the Main thermal fault is hydraulically tight.

The thermal springs originate from small faults and fractures in the Upper Carboniferous sedimentary rocks in the hanging wall of the Main thermal fault, i.e. SE of this fault. Bilharz (1934) proposed a high-angle, NW-trending minor fault connecting the springs Höll-, Mur-, and Fettquelle with each other. Figure 6 shows

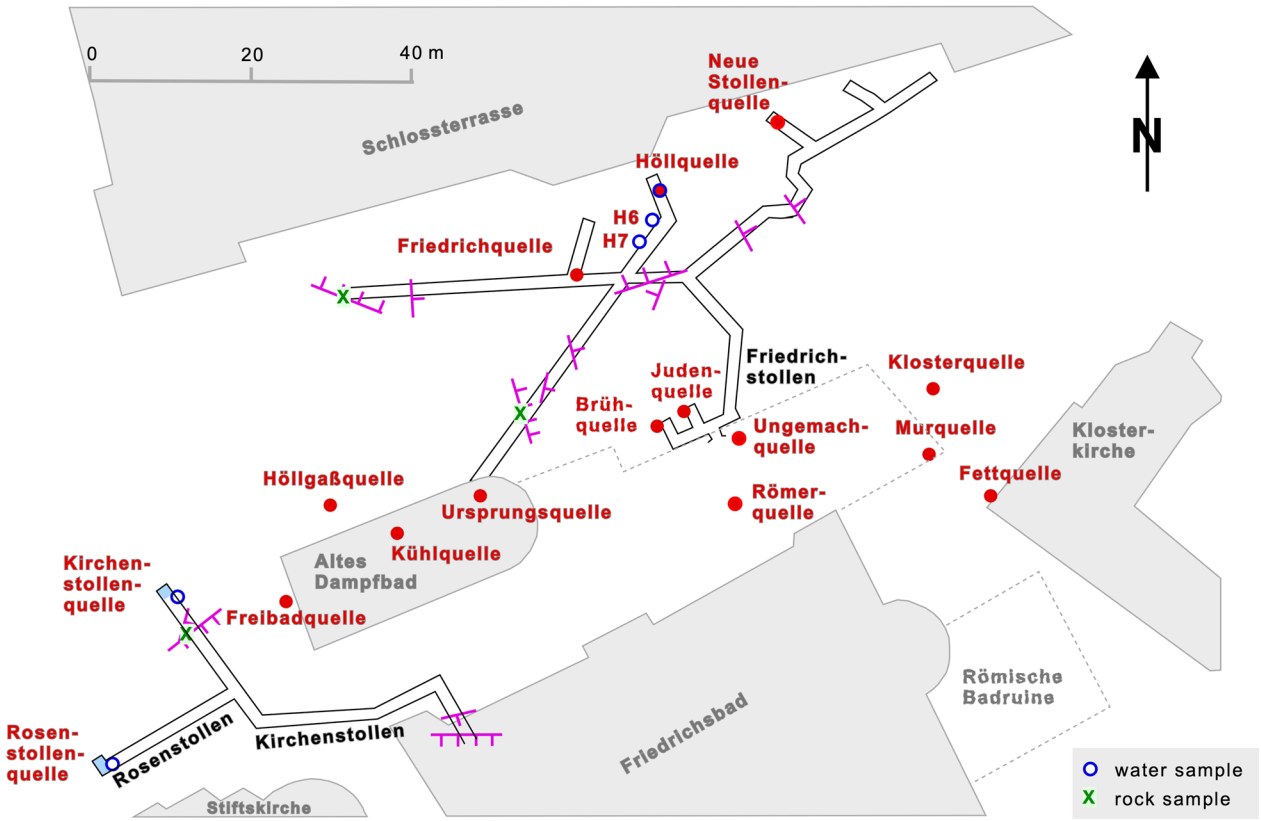

Fig. 6 Location of the thermal springs (Quelle) within the two galleries: Friedrichstollen and Kirchenstollen. Additionally, not accessible springs are shown. The name of the springs is marked in red color. 'Blue circles' show the location of spring water samples, collected within this study, in 'green': locations, where rock samples were taken, and in 'violet': locations and orientation data of faults and strata. Friedrichsbad is one of the local thermal spas, nearby the relics of the former Roman spa ("Römische Badruine"). Ground plan of the tunnel system after Kirchheimer (1959)

the location of the thermal springs within the two branched gallery system, the Friedrichstollen and the Kirchenstollen, and outside of the galleries. However, some of the latter are partly no longer accessible or do not exist anymore. During sampling in March 2022 the two springs Friedrichsquelle and Neue Stollenquelle were dry, but two new thermal springs H6 and H7, nearby the Höllquelle, have developed (Fig. 6). The springs Judenquelle and Brühquelle within the Friedrichstollen were not accessible for sampling.

4.3.1.2 Thermal wells Additionally, thermal water for the spa of Baden-Baden is produced from two wells (Florentinerquelle I and II) about 150 m N of the Friedrichstollen (not shown in Fig. 6). The two wells, drilled and completed between 1966 and 1969, reach a depth of 301.5 m and 553.0 m respectively. Florentinerquelle I (200.4 m NN) was drilled as inclined well, is oriented in S direction and reached its final depth about 20 m E of the New Castle of Baden-Baden. The castle terrace can be seen in the upper part of Fig. 6. Florentinerquelle II (200.4 m NN) is a vertical well, about 5 m E of the inclined well. Both boreholes penetrated below few meters first into the Friesenberg granite, then crossed the Friesenberg fault, a WSW to ENE oriented thrust fault, in 228 m, resp. 358 m depth. This fault-zone is about < 29 m, resp. 16 m, thick and consists of an alternating sequence of thin (cataclastic) slices of metamorphic schists, described as quartz-muscovite-chlorite-schists, and granite. Below this fault zone, the metamorphic schists are present in both boreholes until the bottom of the wells (Maus & Sauer, 1972).

The Friesenberg granite intruded during the Lower Carboniferous. Subsequent extensional movements in the Upper Carboniferous and Lower Rotliegend led to the collapse of pull-apart basins, i.e. deep basins that were filled with the debris of the rising rock and later during the Rotliegend with volcanic material and fanglomerates (Thuro, 1998). However, the contact between Friesenberg granite and the metamorphic schists exhibits no contact metamorphic mineral assemblages; the reverse fault presents a structural contact between granite and metamorphic schists (Sittig, 1965, Maus & Sauer, 1972). In the Michaels-Tunnel the Friesenberg granite in vicinity of the fault-zone is described as mylonitic granite (Fig. 3).

Both boreholes have tapped at various depths artesian thermal water flowing freely out above ground.

Evaluation of former flowmeter-Logs in the inclined and at that time uncased, artesian borehole Florentinerquelle I document, that inflow and even outflow from fractures or minor faults occurred exclusively within the Friesenberg granite. However, inflow prevails with the main inflow at 182 to 185 m and a smaller inflow at 188 to 196 m depth. No flow occurred in the c. 44 m thick metamorphic schists, the reverse fault, and in the Friesenberg granite above 179 m (measured depth, MD). Temperature-Logs are compatible with flowmeter data, i.e. in- and/or outflow of hotter or cooler water in the Friesenberg granite, but no temperature disturbances occur within the metamorphic schists, the reverse fault, and in the Friesenberg granite above 134 m MD. Maximum temperature at the deepest point of measurement (301 m MD) was 70.2 °C. Thus, this borehole only extracts thermal water from the Friesenberg granite in the hanging wall of the reverse fault, and the Friesenberg granite seems to be more or less tight in its upper part (≤ 134 m MD). This means, that the Friesenberg granite above and in the vicinity of the reverse fault developed a hydraulically permeable damage zone, whereas farther away from the reverse fault the granite is relatively impermeable.

Inflow in the well Florentinerquelle II occurs, according to Maus and Sauer (1972), from fractures in the Friesenberg granite at 139 m, but additionally from fractures in the metamorphic schists at different depths below 446 m, whereas the main inflow into the well was observed in 496.6 m depth. Own evaluations of old temperature-Logs in the at that time uncased and only 482 m deep borehole showed possible inflow from the granite below 125 m depth, but not within the fault zone, and a small possible inflow from the metamorphic schists at 456 m depth. Maximum temperature of 62.7 °C was measured in 482 m depth.

4.3.2 Hydrochemical characterization of the thermal waters

The thermal waters were investigated in different laboratories and the oldest analyses date back to the nineteenth century. Table 2 ESM shows the hydrochemical analyses (mg kg^{-1}) of the thermal springs and the thermal wells (Florentinerquelle I, II). The table contains time series (source of data: Carlé, 1975, Bender, 1995, Stober & Bucher, 1999b, Bucher & Stober, 2000, Käß & Käß, 2008, Bons et al., 2014, Sanjuan et al., 2016, old unpublished data from labs: UIS—Umweltinstitut synlab GmbH, UMLAB, University of Freiburg, our investigations: samples taken 2022). The last sample in the table (Friedrichstollen 11.08.2011, taken by Sanjuan et al., 2016) is most probably from the merged springs Brüh-, Ungemach-, and Judenquelle. In 2022, when we collected water samples, the two springs (Friedrichsquelle, Neue Stollenquelle) were dry and two new thermal springs (H6, H7) occurred.

The composition of all thermal waters changed in time, but the Na-Cl-dominated water type has always been identical, as shown as an example for the spring Friedrichsquelle (Fig. 7A, B). Total dissolved solids

(TDS) in the Friedrichsquelle changes in the course of time (1891–2021) between 2690 mg kg^{-1} and 3130 mg kg^{-1} (Table 2 ESM). During our sampling in May 2022 the spring was dry. The Schoeller-Diagram in Fig. 7B shows that the water type of the Friedrichsquelle did not change in time, despite fluctuations of TDS* (= TDS–SiO_2) (Fig. 7A). Drilling of the two boreholes, Florentinerquelle I and II, in 1965–1967 might have caused a decrease of TDS* in the Friedrichsquelle. A hydraulic connection between Florentinerquelle I and Friedrichsquelle is documented (unpublished files of the Environmental Agency Baden-Baden). During the construction of the Michaels-Tunnel (1980–1989) TDS* in the Friedrichsquelle remained constant (Fig. 7A), despite a significant decrease of the flow rate (Carasana 2004). TDS* of the two thermal wells Florentinerquelle I and II seems to have decreased because of the construction of the Michaels-Tunnel, but years later TDS* increased again.

Generally, it can be assumed that the thermal springs react to heavy precipitation with a decrease in TDS*, as shown by sporadically measured NO_3 concentrations. Further hints on dilution of the thermal spring water by precipitation can be derived from isotope studies (see chap. 4.4).

Not all fluctuations in TDS of the thermal springs can be explained, since our knowledge on subsurface interventions and thereby possibly caused contamination by surface water is incomplete. Generally, it cannot be excluded that the fluctuations in TDS of some or even all thermal springs are (additionally or partly) caused by natural processes, such as minor dilution with meteoric water or with other thermal waters nearby, having lower TDS. The fact that some springs became inactive and others newly emerged also suggests near surface processes. Obviously, upwelling thermal water sometimes must use other or additional flow paths, as older ones become sealed or blocked because of precipitation of minerals from supersaturated waters or deformation and (micro-)seismic events. Generally, in the Friedrichstollen the discharge rate of the topographically lower situated springs increased in the last 100 years at the expense of topographically higher situated springs. Additionally, Käß (1995) observed a decrease of productivity in the boreholes Florentinerquelle I and II by half since initial operation. The discharge rate of the thermal springs in the Friedrichstollen decreased slightly from about

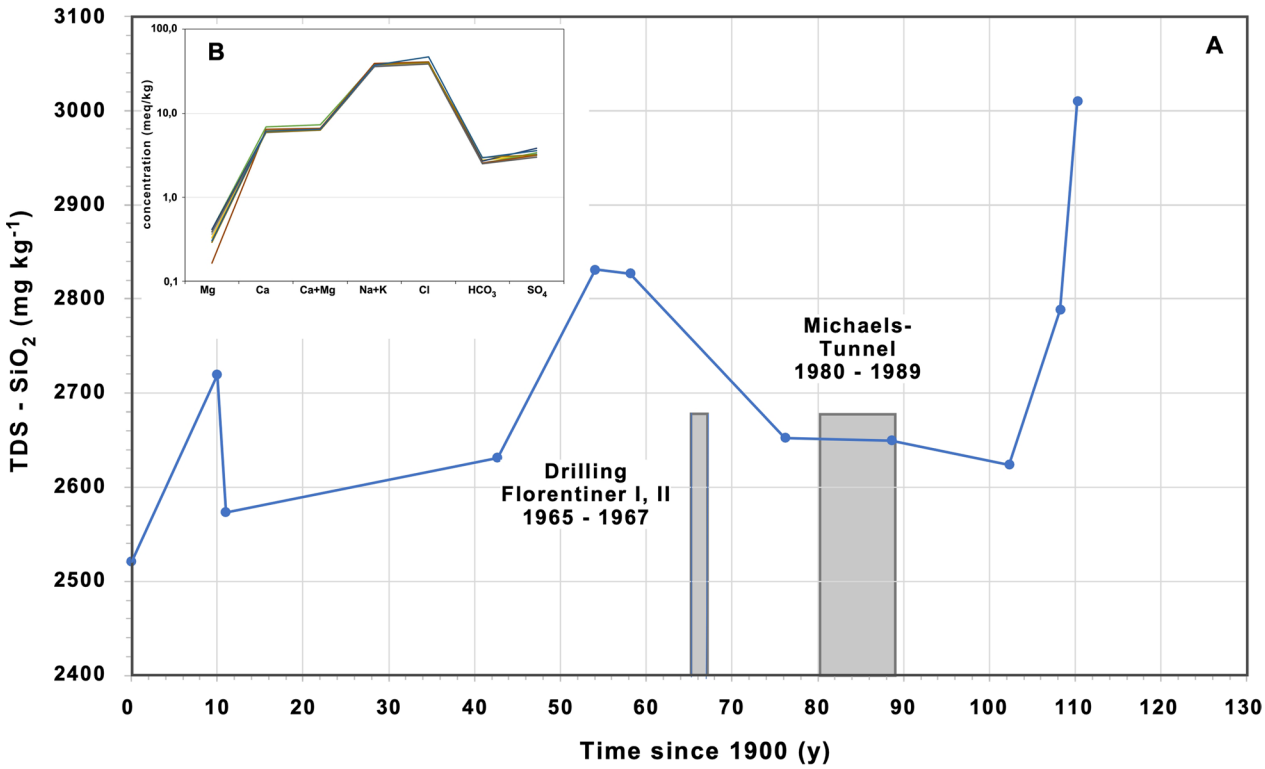

Fig. 7 **A** Example of hydrochemical fluctuations in thermal spring waters of the Friedrichsquelle (Fig. 6). Since SiO_2 was determined with different methods and partly indicated implausible values, the y-axis shows instead of TDS the term TDS* (TDS–SiO_2). **B** The Schoeller-Diagram of all analyses of the Friedrichsquelle shows the constant water type

7.6 to 6.8 L s^{-1} since production from the boreholes started, whereas the Friedrichsquelle hydraulically reacts significantly to increased production-rates of the borehole Florentinerquelle I (Schrage, 2004). In any case, the thermal water system appears to be very dynamic and some thermal springs and even thermal wells are hydraulically interconnected with each other.

In the following, we focused mainly on recent analyses of the thermal springs and the wells Florentienerquelle I and II and on some few older analyses of springs, which do not longer exist or were not accessible, i.e. we focus on a selection of the compiled analyses, listed in Table 2 ESM. However, these thermal waters were collected from different institutions and analyzed in different laboratories. Nevertheless, there are quite a lot of similarities.

The arithmetic mean (abbreviated with mean value throughout the text) of temperature is T = 60 °C (δ = 8.5 °C). The lowest temperature was measured in the Rosenstollenquelle (T = 41.2 °C), situated in the Kirchenstollen (Fig. 6) and the highest temperature in the Höllquelle (T = 69.0 °C). Temperatures of the thermal waters of the wells Florentinerquelle I and II (58.4 °C, 53.6 °C) were measured at the well head and showed generally lower values than thermal spring waters in the Friedrichstollen (> 63 °C). Lower temperatures are probably (or additionally) caused by low production rates in combination with longer ascend paths within the wells (Fig. 8.9 in Stober & Bucher, 2021). The mean value of pH is 7.25 (δ = 0.24), but it needs to be taken into account that probably not all pH-values were measured in situ but in the laboratory at lower temperatures. For example, Sanjuan et al. (2016) and Göb et al. (2013) measured pH in any case as well as in situ.

Figure 5B shows the main components of these selected thermal waters in a Schoeller-Diagram. The water type of all thermal waters (springs, boreholes) is practically identical. Na and Cl are the dominant water components. Mean values of the main components are: Na = 847.9 mg kg^{-1} (δ = 65.5), K = 82.3 mg kg^{-1} (δ = 8.4), Ca = 120.5 mg kg^{-1} (δ = 7.8), Mg = 5.0 mg kg^{-1} (δ = 2.8), Cl = 1458.1 mg kg^{-1} (δ = 148.2), HCO_3 = 181.4 mg kg^{-1} (δ = 27.5), SO_4 = 156.4 mg kg^{-1} (δ = 9.8).

The thermal waters differ somewhat in total dissolved solids (TDS). The highest concentration TDS* = 3261 mg kg^{-1} of the selected thermal waters was measured in the thermal well Florentinerquelle II and the lowest with TDS* = 2425 mg kg^{-1} in the thermal well Florentinerquelle I (Fig. 5B, Table 2 ESM). Concentration of the thermal springs is between TDS* = 2537 mg kg^{-1} (Ursprungsquelle) and TDS* = 3053 mg kg^{-1} (Murquelle). SiO_2 in the thermal spring waters varies between 116 and 137 mg kg^{-1}.

The mean value of Na/Cl molar ratio of the thermal waters is Na/Cl = 0.90 with a relatively low standard deviation (δ = 0.08). Contrarily, the waters in the Michaels-Tunnel scatter much stronger. However, in the central part of the tunnel (samples no. 6–11, Table 1 ESM) Na/Cl ratio is more or less equal to those of the thermal waters. Na/Cl of modern seawater is lower (0.86) (Stumm & Morgan 1975).

X_{Na} = Na/(Na + Ca) (molar ratio) of selected thermal waters, i.e. spring- and thermal water of wells, are nearly identical to the mean value X_{Na} = 0.860 (δ = 0.008) (Fig. 8). Contrarily, X_{Na} of the waters in the Michaels-Tunnel scatter strongly. However, in the central part of the tunnel (samples no. 6–12, Table 2 ESM) X_{Na} is significantly higher, and the mean value of these water samples X_{Na} = 0.803 (δ = 0.018) is only somewhat lower than that of the thermal waters (Fig. 8). The constant X_{Na} = Na/(Na + Ca) = 0.86 in particular of all thermal waters also speaks for the origin of the waters from granites, i.e. for plagioclase cation exchange with an aqueous solution at enhanced temperatures. X_{Ab} (= $a_{Ab}/(a_{Ab} + a_{An})$) of plagioclase in the biotite-granite of Baden-Baden is lower and about X_{Ab} = 0.792 (Table 4 ESM) as X_{Na} of the thermal waters, which is in agreement with investigations of Orville (1972). Theoretically, assuming fully equilibration of plagioclase with the hot fluid, X_{Na} of the fluid is increasing with increasing X_{Ab} of plagioclase. Additionally, X_{Na} of the fluid is temperature dependent and increases with increasing temperature.

Trace elements were only measured in thermal waters (Table 2 ESM), i.e. not in water samples of the Michaels-Tunnel. The mean value of fluoride concentration is F = 4.72 mg kg^{-1} (δ = 1.48), of lithium Li = 8.72 mg kg^{-1} (δ = 0.55), and of strontium Sr = 2.88 mg kg^{-1} (δ = 0.50) (Fig. 9A). Particularly, the scatter of both Li and Sr is very low. The difference between mean- and median values is very small. The Ca/Sr, Ca/F, and Na/Li mass ratios are close together in each case and the mean values correspond to Ca/Sr = 44.0 (δ = 9.0), Ca/F = 24.8 (δ = 4.6), and Na/Li = 97.5 (δ = 5.5).

Variance of arsenic is also very low and with a mean value of As = 0.204 mg kg^{-1} (δ = 0.013) it is well above the limit value of the drinking water ordinance (Fig. 9B). Barium in the thermal waters is low with Ba = 0.146 mg kg^{-1} (δ = 0.024) as mean value. Contrarily to the other trace elements the standard deviation of iron is quite high: mean value Fe = 0.127 mg kg^{-1} and δ = 0.071 (Fig. 9B). Mean value of manganese in the thermal waters is Mn = 0.42 mg kg^{-1} with a low standard deviation (δ = 0.05) (Table 2 ESM).

Thus, not only the main components of the thermal waters of Baden-Baden are very similar but also the

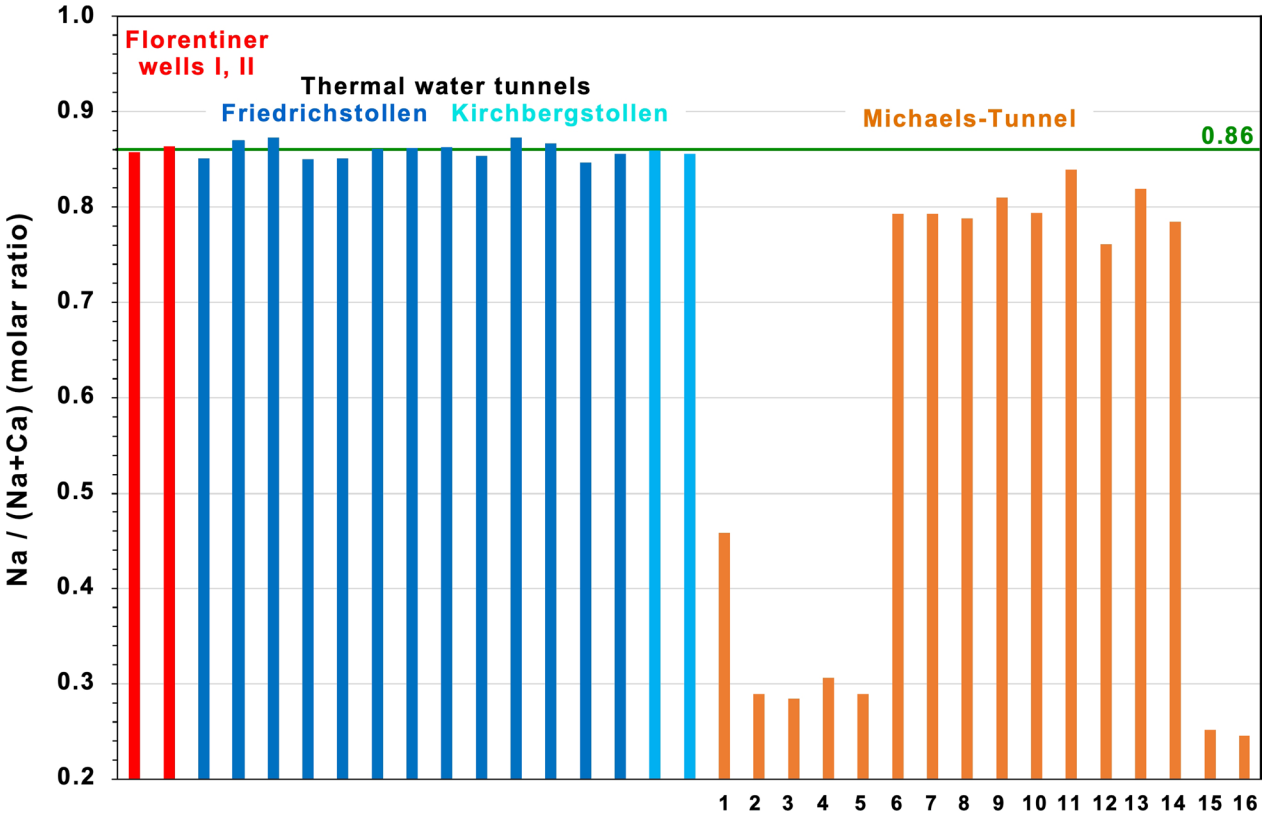

Fig. 8 X_{Na} = Na/(Na + Ca) (molar ratio) of thermal waters from the wells Florentinerquelle I and II (red), the thermal springs (dark and light blue) and waters collected in the Michaels-Tunnel section (orange) (Tables 2, 1 ESM). Numbers on the x-axis refer to the water samples taken in the Michaels-Tunnel (Table 1 ESM, Fig. 3)

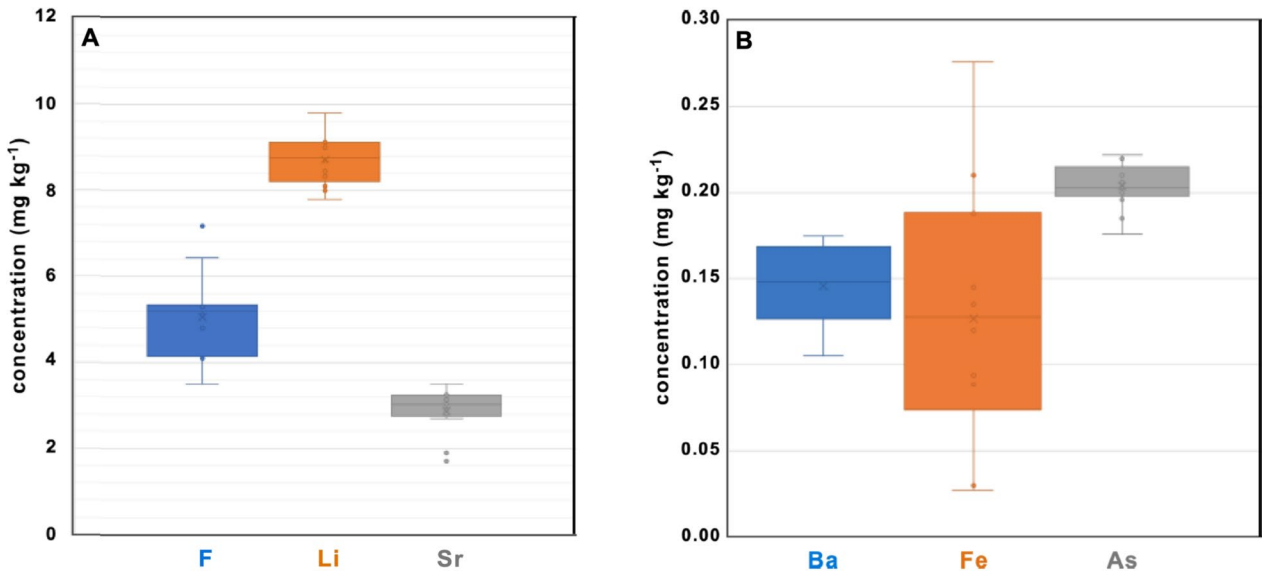

Fig. 9 Box-Whisker-Plots of selected trace elements from thermal waters. **A** fluoride-, lithium-, and strontium concentration, **B** barite-, iron-, and arsenic concentration in thermal waters of the springs and the wells Florentinerquelle I and II. Median values are presented as 'horizontal lines' within the boxes and arithmetic means are marked with a 'cross'

trace elements, even though the thermal waters were analyzed in different laboratories at different times and though they flow out from different geological units (i.e. Friesenberg-granite, metamorphic schists, Upper Carboniferous sediments). Thus, it is highly likely that the thermal springs (and the thermal waters of the wells) have the same origin and that they are upwelling along fractures and faults from the deep reaching, fractured granite into overlaying fractured Upper Carboniferous sediments and metamorphic schists.

4.3.3 Saturation state of the thermal waters

The hydrochemical development of the waters was modeled with the computer program PHREEQC (Parkhurst & Appelo, 1999) using the LLNL thermodynamic database (Lawrence Livermore National Laboratory, 2020). Saturation indices (SI) of the thermal waters with respect to selected minerals were determined, whereas $SI < 0$ indicates undersaturation, $SI = 0$ saturation and $SI > 0$ supersaturation with respect to a certain mineral. Minerals can possibly precipitate if water is saturated or supersaturated.

Based on PHREEQC calculations, thermal waters are supersaturated with respect to quartz (mean value $SI_{Qtz} = 0.80$, $\delta = 0.10$), calcite (mean $SI_{Cal} = 0.38$, $\delta = 0.25$), aragonite (mean $SI_{Ara} = 0.24$, $\delta = 0.25$), and dolomite (mean $SI_{Dol} = 0.85$, $\delta = 0.47$). Supersaturation with respect to quartz indicates that all thermal waters originate from a reservoir in greater depth with much higher temperatures. Supersaturation with respect to the carbonate minerals might be caused by degassing during upwelling of the thermal waters as a result of pressure reduction and due to comparatively lower atmospheric CO_2-pressure, which is consistent with the rather low pH values.

Despite $SI_{Dol} > SI_{Cal}$, dolomite may not precipitate from the thermal waters for kinetic reasons including very high activation energy for nucleating crystals of dolomite (Blatt & Tracy, 1996). According to Walenta (1992) calcite frequently occurs in hydrothermal veins in granitic rocks of the Schwarzwald, whereas dolomite is less common and has incorporated iron, maybe as nucleating crystals. Historically it is a known, that after the Romans left the thermal springs, a several meters thick sinter mound formed from the free-flowing thermal springs, consisting mainly of aragonite and, to a lesser extent, of calcspar and siliceous sinter (Beyer, 1788). These findings are in agreement with the PHREEQC calculations. Original sinter material is still accessible at the grotto of the thermal spring Fettquelle (Fig. 10).

Generally, the thermal waters are undersaturated with respect to the sulfate minerals anhydrite (mean $SI_{Anh} = -1.38$, $\delta = 0.10$) and gypsum (mean $SI_{Gyp} = -1.52$, $\delta = 0.04$), influenced by the retrograde solubility (for gypsum: temperature > 35 °C). Thus, no precipitation of these minerals is to be expected and accordingly is not observed. Contrarily, all thermal waters are more or less saturated with respect to barite (mean $SI_{Bar} = 0.03$, $\delta = 0.09$) (Fig. 11), indicating that precipitation of barite might occur. However, barite is a wide distributed fracture-filling mineral in the Schwarzwald.

All thermal waters are strongly supersaturated with respect to iron (Fe) oxides, like hematite or goethite, indicating potential precipitation of these minerals. Hematite or goethite are usually formed secondarily by alteration of Fe-minerals like magnetite or pyrite, whereas e.g. in deep fluids alteration of magnetite uses H_2O as oxidizing agent to produce hematite (e.g. Bucher, 2023). Fe-oxides like hematite or goethite are common and widespread fissure minerals in granitic rocks of the Schwarzwald (e.g. Walenta, 1992). Sulfide (e.g. pyrite,

Fig. 10 Sinter material at the Fettquelle, composed mainly of aragonite and, to a lesser extent, of calcspar and siliceous sinter

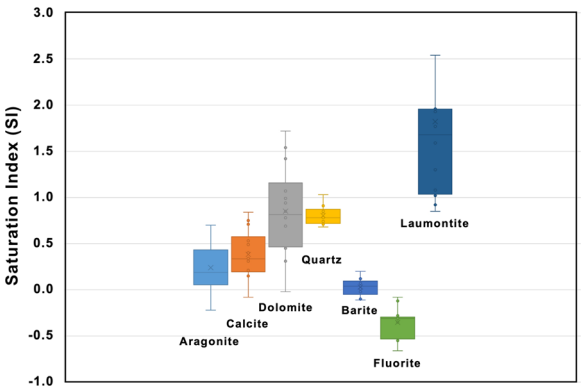

Fig. 11 Box-Whisker-Plot of the Saturation Index (SI) with respect to selected minerals in the thermal waters. Median values are presented as 'horizontal lines' within the boxes and the arithmetic mean is marked with a 'cross'

FeS_2) weathering and oxidation of sulfur—in detail described in Stober and Bucher (2010, Eqs. 2 and 4)—is the major source of SO_4 in thermal waters in a granitic surrounding (Fig. 5B) causing supersaturation with respect to Fe-oxides, e.g. goethite (Stober & Bucher, 1999b). An additional source of Fe could be alteration of biotite in the granites south and in the subsurface of Baden-Baden.

The thermal waters are as well supersaturated with respect to clay minerals like kaolinite, illite, or montmorillonite, widespread alteration products found in the Schwarzwald basement rocks, and they are supersaturated with respect to zeolites like laumontite (mean $SI_{Lau} = 1.82$, $\delta = 1.06$), heulandite, analcime, or stilbite. According to Walenta (1992) zeolites are among the lesser common minerals in granitic rocks of the Schwarzwald, with laumontite being the most usual member, but the occurrence of analcime and stilbite is as well documented in crystalline basement rocks of the Schwarzwald. All thermal waters are as well supersaturated with respect to sheet silicates like beidellite or muscovite.

Saturation Indices of selected minerals are shown in Fig. 11 as Box-Whisker-Plots. Equally, the saturation indices of the thermal waters of Baden-Baden are very similar, although these waters emerge from different geological units (i.e. Friesenberg-granite, metamorphic schists, Upper Carboniferous sediments). The saturation indices indicate as well that the thermal waters had a long-lasting contact time with granitic rocks and were shaped there by their long residence time before entering overlaying strata like Upper Carboniferous sediments or metamorphic schists with no visible impact on hydrochemistry.

4.3.4 Estimating reservoir temperature from the composition of deep fluids

The chemical composition of deep fluid reflects the temperature of the geothermal reservoir. The equilibrium fluid composition is unique for the reservoir rock and the *P–T* conditions at the reservoir. Therefore, the reservoir temperature can be deduced from the fluid composition if the type of rock dominating the reservoir is known. The temperature at depth can be derived from an empirical calibration or from computed equilibrium conditions using thermodynamic models and data. An empirical calibration correlates fluids from a known rock type with measured temperatures from the fluid sampling depth in deep wells. Within this article we used as well thermodynamic models of two widely used geothermometers (SiO_2, Na/K). Inference of a meaningful reservoir temperature from temperature—composition relationships is fundamentally based on the assumption of chemical equilibrium of a considered chemical fluid-rock reaction (Stober & Bucher, 2021).

4.3.4.1 Quartz-geothermometry Quartz is an abundant mineral in many reservoir rocks. The solubility depends predominantly on temperature, while the influence of pressure is negligible. The SiO_2 geothermometer is independent of the pH in acid and neutral fluids. In high-pH fluids the solubility of quartz rapidly increases with increasing pH. The silica geothermometer is vulnerable to dilution by low-silica surface waters and to precipitation of solid SiO_2 along the ascent path. However, reaction kinetics of quartz formation is slow and during cooling the fluid remains oversaturated with quartz. Therefore, calculated reservoir temperatures for thermal springs are minimum temperatures.

The SiO_2 concentrations in the thermal springs Murquelle, Rosenstollenquelle, Friedrichquelle, Kirchstollenquelle, and Höllquelle of Baden-Baden are close to each other and fluctuate between 116.25 and 130.00 mg kg^{-1} (Table 2 ESM). We used the quartz-geothermometers of different authors (Fournier, 1977, Walter & Helgeson, 1977, Fournier & Potter, 1982, Arnórsson, 1983, Verma, 2000, Stober & Bucher, 2021) to calculate reservoir temperature (Table 3 ESM). Generally, these geothermometers are based on empirical calibrations (correlations), while the geothermometer of Stober and Bucher (2021) calculates the temperature based on the equilibrium conditions for quartz solubility by using the computer program SUPCRTBL (Zimmer et al., 2016) with data for the solids (Holland & Powell, 2011).

The geothermometer of Arnórsson (1983) provided the lowest temperatures and the highest temperatures were calculated with the geothermometer of Walter and Helgeson (1977). The arithmetic mean of all geothermometers' results of the geothermal springs fluctuates between 143 and 150 °C, indicating more or less the same reservoir depth (Table 3 ESM).

4.3.4.2 Cation-ratio-geothermometry Some geothermometers use cation ratios, like Na/K, Mg/K, Ca/K, Na/Li, rather than absolute concentrations as the quartz geothermometer. Cation-ratio-geothermometers are generally based on empirical calibrations between measured temperatures and cation ratios (e.g. Michard, 1990; Verma & Santoyo, 1997, Can, 2002). In contrast, the cation geothermometers (Na/K, Mg/K) of Stober and Bucher (2021) calculate the temperature based on the equilibrium of the exchange reaction between the corresponding minerals by using the computer program SUPCRTBL (Zimmer et al., 2016) with data for the solids (Holland & Powell, 2011).

4.3.4.3 Na–K geothermometry Cation ratios, like Na/K, are controlled by mainly temperature dependent exchange reactions between minerals and the fluid. Geothermal waters, e.g. residing in crystalline basement formations such as granite or gneiss, are typically in contact with K-feldspar ($KAlSi_3O_8$) and plagioclase normally rich in Na-feldspar component ($NaAlSi_3O_8$).

Although hot groundwater at depths of some km may not be in full chemical equilibrium with the primary minerals of granitoid basement Na/K ratios of this water is dictated by the presence of two primary feldspars (Eq. 1).

$$KAlSi_3O_8 + Na^+(\text{fluid}) = NaAlSi_3O_8 + K^+(\text{fluid}) \quad (1)$$

The T-estimate (°C) of Stober and Bucher (2021) requires the assemblage microcline (low-T K-feldspar, Kfs) and albite (Ab) and is based on Eq. 2.

$$T = \left\{-1216.7/\left(\log\left(c_K/c_{Na}\right) - 1.42125\right)\right\} - 273 \quad (2)$$

where c_K and c_{Na} denote the K- and Na concentration in mg L^{-1} (Table 2 ESM). If the Na–K exchange reaction involves a more general alkali feldspar and plagioclase (oligoclase, andesine), the Na/K-geothermometer must be modified and include a term for the activities of the components albite and K-feldspar (a_{Ab}, a_{Kfs}) in the feldspars (Stober & Bucher, 2021, Stober et al., 2022):

$$T = \left\{-1216.7/\left(\left(\log\left(c_{K+}/c_{Na+}\right)\right.\right.\right. + \left.\left.\left.\left(\log\left(a_{Ab}/a_{Kfs}\right)\right) - 1.42125\right)\right\} - 273 \quad (3)$$

In an ideal solid solution, the activity is simply equal to the mol-fraction. The mean measured compositions for K-feldspar results in $a_{Kfs} = 0.95$ and for plagioclase $a_{Ab} = 0.79$ in the Baden-Baden biotite-granite using a standard state of pure microcline and pure albite at *P–T* (Table 4 ESM).

The Na/K-geothermometers by Can (2002) and Verma and Santoyo (1997) lead to reservoir temperatures significantly higher as the minimum reservoir temperature calculated by quartz-geothermometry (Table 3 ESM). While the geothermometer of Can (2002) shows reservoir temperatures slightly above 200 °C, the one of Verma and Santoyo (1997) leads to reservoir temperatures of c. 216 °C. Contrarily the Na/K-geothermometer of Stober and Bucher (2021), based on the equilibrium of the exchange reaction between the corresponding minerals -assuming ideal Kfs and Plg composition-, leads to slightly higher temperatures (Table 3 ESM). Taking into account the actual composition of K-feldspar and plagioclase (Tab. 4 ESM, Eq. 3) reservoir temperature is calculated to about 210 °C, assuming equilibrium between the involved feldspars is reached.

4.3.4.4 Giggenbach triangle-geothermometer A particularly widely used ternary diagram for geothermal fluids has been devised by Giggenbach (1988). Measured concentrations of Mg, K, and Na are shown on a ternary plot together with the empirically derived data points for 'fully equilibrated water' at temperatures ranging from 80 to 300 °C (Fig. 12). In a geothermal reservoir at depth infiltrating meteoric water evolves, according to Giggenbach (1988), from the Mg corner through a field of 'immature waters' and later through a field of 'partially equilibrated waters' to 'mature waters' before reaching the curve of full equilibration. The waters collected from the thermal springs and thermal wells of the geothermal field tend to define an evolution line, that points towards a temperature on the 'full equilibration curve'. This temperature is thought to represent the reservoir temperature.

The Giggenbach diagram is based on two temperature sensitive reactions: the two primary feldspars (albite, K-feldspar) determine the K-Na-exchange (Eq. 1) and the alteration assemblage phengite (white mica) and chlorite for the Mg–K-exchange, which at equilibrium requires equilibrium of the Al-balanced reaction: phengite (white mica) + chlorite + quartz = K-feldspar (Eq. 4):

$$8\,KAl_3Si_3O_{10}(OH)_2 + 2\,Mg_5Al_2Si_3O_{10}(OH)_8 + 54\,SiO_2 + 20\,K^+ = 28\,KAlSi_3O_8 + 10\,Mg^{2+} + 16\,H_2O \quad (4)$$

The well-developed and rapidly established K-Na equilibrium causes the water composition from very many reported geothermal fields to lie on a linear array

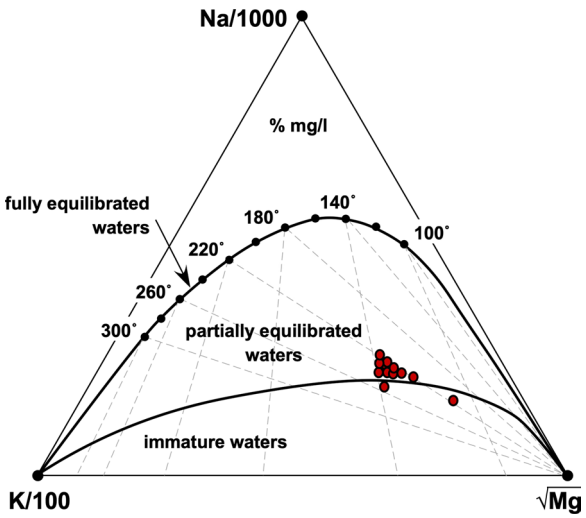

Fig. 12 Giggenbach-diagram showing the geothermal waters of Baden-Baden on an evolution path towards an estimated reservoir temperature of 220 °C

simply reflecting the K-Na equilibrium temperature (Eq. 2). The linear array intersects the curve 'fully equilibrated waters' (Fig. 12) where the fluid would be in equilibrium with chlorite, phengite and K-feldspar in the granitic reservoir rocks. Most hot waters, however, do not represent full Mg–K equilibrium with altered granite. According to the Giggenbach-diagram the reservoir temperature is estimated to T = 220 °C, comparable to results in Table 3 ESM.

4.3.4.5 Isotope-geothermometry The measured oxygen isotope composition of the dissolved sulphate (Tables 5 ESM) and the water (Friedrichsen, 1981; Bender, 1995) allow to calculate an independent reservoir temperature if equilibrium had been achieved. Table 5 ESM shows calculated reservoir temperatures using different methods. Depending on the investigation method the temperature rage is wide and scatters between c. 120 and 190 °C.

4.4 Results of isotope analyses

The isotope values are useful to trace the origin of the thermal water and its solutes as well as allow to constrain the flow path of Baden-Baden fluid.

The sulfur and oxygen isotope composition of the dissolved sulfate is presented in Table 6 ESM and illustrated in Fig. 13A. The fluid data excludes dissolution of marine evaporitic sulfate (Strauss, 1997) like gypsum or anhydrite as well as atmospheric non-sea-salt sulfate e.g. from oxidation of dimethyl sulfide (CH_3SCH_3), making it very likely that oxidation of sulfides in the crystalline basement is the most probable source of SO_4 in the fluid (see also e.g. Pastorelli et al., 2001; Bucher et al., 2009a, 2009b). An abiotic sulfide oxidation is also indicated by the range of $d^{18}O_{SO4}$ and $d^{18}O_{H2O}$ values (Boschetti, 2013).

The water isotope composition and tritium concentrations are compiled in Table 7 ESM and displayed in Fig. 13B. The high tritium concentration in 'Neue Stollenquelle' is most probably caused by admixed rainwater intruding the gallery via a vertical ventilation shaft. Heavy rainfalls prior and at the sampling day are documented by the DWD (Deutscher Wetterdienst, German meteorological service) during the period 18.-24.03.2002. Thus, in accordance with the hydrochemical investigations (Figs. 5, 7, sporadically measured NO_3 concentrations) infiltration of rainwater occurs shifting the water isotope data to higher values. Figure 13C shows that the thermal waters don't result from a mixing between deep geothermal brines (as those from Insheim, Bruchsal, Soultz, Rittershoffen, etc. in the URG).

The water isotope composition indicates that the Baden-Baden fluid consists of meteoric water without any seawater component. There are also no indications for isotope shifts based on other processes like evaporation, CO_2 exchange, or low-temperature fluid-rock interaction.

Water isotope data can additionally be used for pinning down the recharge elevation (Fig. 13D), assuming that climatic conditions during the time of infiltration were similar. The recharge elevation of Baden-Baden thermal springs is estimated as indicated by the red arrow in Fig. 13D. Please note that at least the Baden-Baden data point with the heaviest $d^{18}O$ value is influenced by mixing with rainwater at the low elevation of the thermal springs in Baden-Baden (Table 7 ESM). Therefore, the highest and most reliable recharge elevations (red arrow in Fig. 13D) are from the thermal springs Friedrichsquelle (932 m) and Höllquelle (924 m) and from the thermal well Florentinerquelle I (920 m). The resulting mean elevation of 884 ± 35 m (1 STD; excluding 'Neue Stollenquelle') indicates a recharge area just below (north of) the 'Badener Höhe' (1002 m a.s.l.) where the basement is covered with Buntsandstein (Fig. 1).

The strontium isotope composition is shown in Fig. 13E. Variable strontium isotope signatures of fluids most probably do not reflect different source rocks but can be linked to specific local mineral breakdown reactions dominating during distinct fluid-rock interaction stages (Glodny et al., 2009). A high strontium isotope ratio ($^{87}Sr/^{86}Sr$) from the early low-temperature stage of fluid-rock interaction points to biotite breakdown in a granitic environment as a major source of solutes in the fluids of Baden-Baden, whereas the late high-temperature stage with comparably low $^{87}Sr/^{86}Sr$ ratios can be correlated with dominant feldspar alteration. The latter case is represented by the deep high-temperature fluids in the central URG (Soultz-sous-forêts, Rittershoffen, Landau, Insheim). The temperature dependent mineral breakdown reactions have been confirmed by Drüppel et al. (2020) in hydrothermal experiments at 70 °C (interaction of biotite and minor feldspar with meteoric water), and mainly dissolution of feldspar by brines at 200 °C.

Noble gases of Baden-Baden fluids have been analyzed by Grieshaber et al. (1992) and Bender (1995). The atmospheric noble gas (Kr and Xe) abundances in the fluid can be used to determine the infiltration temperature in the recharge area (e.g. Seltzer et al., 2021) and leaded to temperatures of 5–6 °C (Bender, 1995). The water isotope composition (mean value: $d^{18}O$ – 9.77 ‰; dD – 67.76 ‰, excluding the rainwater influenced 'Neue Stollenquelle') also indicates groundwater recharge during relatively warm climate conditions in the Holocene (van Geldern et al. 2014).

The helium isotope composition is shown in Table 8 ESM and Fig. 13F. The crustal helium isotope

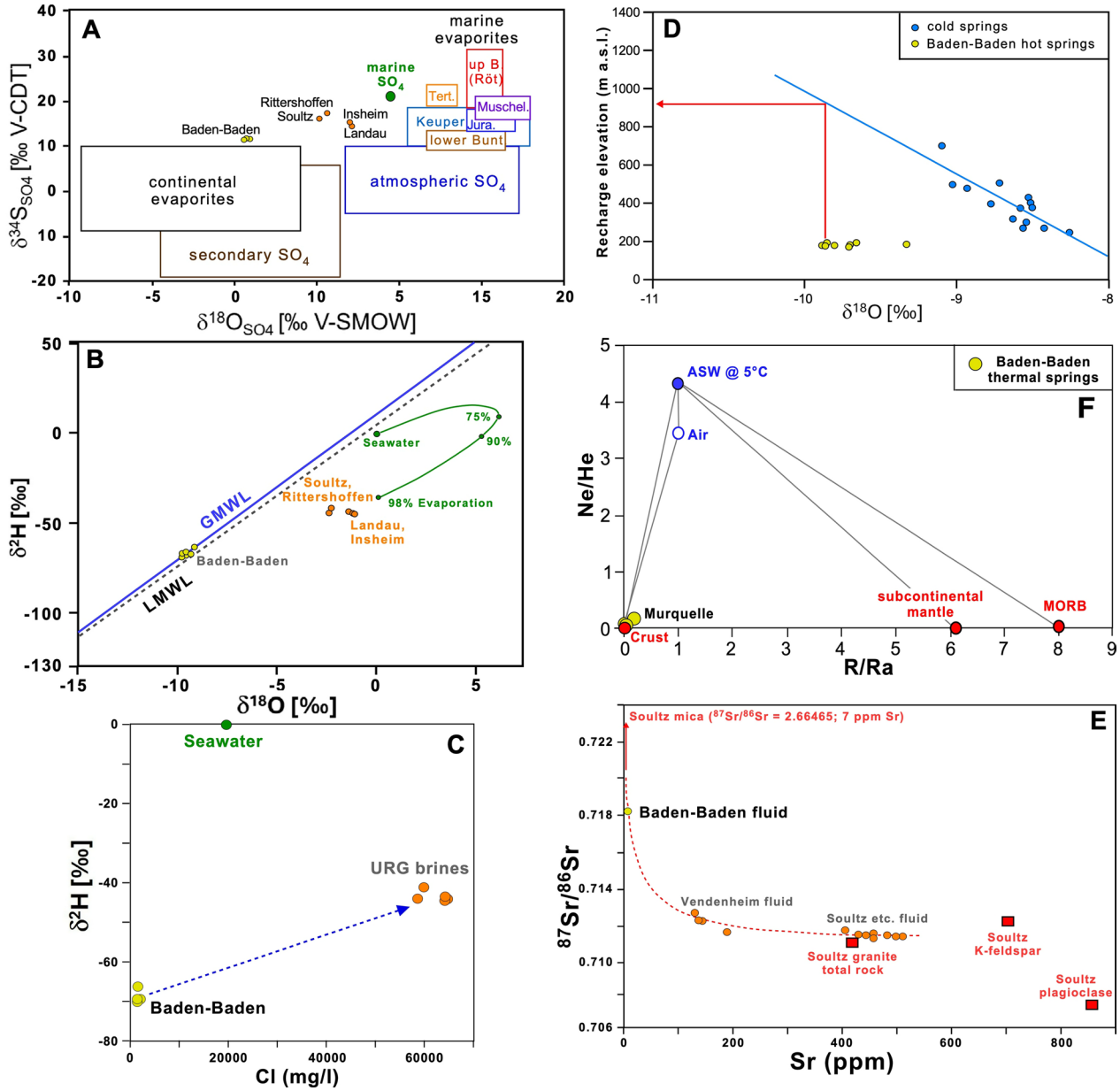

Fig. 13 **A** Sulfur versus oxygen isotope composition of the dissolved sulfate (data from Table 6 ESM). The boxes with the value ranges are mainly taken from Grimm et al. (2005). The data from deep URG fluids (red dots) are from Sanjuan et al. (2016). **B** Oxygen versus hydrogen isotope composition of Baden-Baden thermal spring waters (data from Table 7 ESM). For comparison the deep URG fluids are also plotted (data from Sanjuan et al., 2016). GMWL = Global Meteoric Water Line; LMWL = Local Meteoric Water Line. **C** Chloride (Cl) concentration vs. hydrogen isotope composition of Baden-Baden thermal spring waters, seawater and deep brines from the URG. **D** Emanation elevation versus oxygen isotope values (data from Table 7 ESM and cold springs from Ambs, 2002). **E** Strontium isotope composition versus strontium concentration in fluids and related basement rocks/minerals (data from Sanjuan et al., 2016, 2021 and Aquilina et al., 1997). The Baden-Baden data are shown in 'yellow'. The 'orange dots' include data from deep fluids in the URG (geothermal wells of Soultz-sous-forêts, Rittershoffen, Landau, and Insheim). The 'orange dots' of the deep Vendenheim fluid in the URG contains surface water caused by stimulation activities. **F** Ne/He versus air-normalized $^{3}He/^{4}He$ ratio (R/Ra) of Fett-, Mur-, and Ursprungsquelle (data from Griesshaber et al., 1992). *ASW* Air Saturated Water

composition indicates a flow path of the infiltrating rainwater through the crystalline basement where the initial atmospheric composition is overwhelmed with crustal helium (^{4}He) because of the decay of uranium and thorium during its residence time in the subsurface. Since Grieshaber et al. (1992) provided 'rounded' noble gas data, it was not possible to exactly reproduce the reported numbers of Table 8 ESM. However, it can be

shown that the Ursprungsquelle is characterized by the highest He concentration of the three analyzed Baden-Baden springs caused by its comparably longest residence time in the basement. The Murquelle is characterized by a minor contribution of atmospheric helium and possibly also a mantle helium (^{3}He) component if the latter cannot be excluded (Table 8 ESM). The apparent mantle helium could be caused by the decay of tritium ($^3H \rightarrow {}^3He$) in the ca. 3% admixed recent meteoric water as deduced from 0.6 TU by Bender (1995; Table 7 ESM). The admixed recent meteoric water would also be responsible for the atmospheric component in the fluid of Murquelle.

The fluids from the two wells Florentinerquelle I and II are tritium-free which indicates no admixture of recent meteoric water and a mean residence time of > 60 years.

Since Bender (1995) also measured the ^{14}C activity (1.67 pmc) and the carbon isotope composition of the 161.5 mg L^{-1} dissolved inorganic carbon ($d^{13}C$ DIC = − 10.07), a reassessment of the mean residence time could be done for Friedrichsquelle. The original calculated apparent ^{14}C age for the mean residence time of Friedrichsquelle (26,500 a; Bender, 1995) was based on the approach of Pearson and Hanshaw (1970) and contradicted the evidence from robust stable water isotope composition of hydrogen and oxygen indicating a Holocene age. For the recalculation of the Bender (1995) data the IAEA/Gonfiantini model was used. The originally CO_2-rich fluid (uptake of soil CO_2 released via root respiration: $d^{13}C$ = − 27 ‰; Cerling et al., 1997) has dissolved ^{14}C-free fracture carbonate of the Buntsandstein and the underlying granite. This dead carbon (with $d^{13}C$ up to − 10.9 ‰; Dezayes & Lerouge, 2019) diluted the ^{14}C concentration in the fluid (dilution factor q = 0.06; $d^{13}C$ of dead carbon − 9.5 ‰). The uncertainty of the resulting ^{14}C age value of 10,800 years is (assuming a very uniform $d^{13}C$ value of the dissolved carbonate of − 9.5 ± 0.1 ‰) even in a 2sigma uncertainty of only 4293 a (1sigma: 2146 a). The applied IAEA model considers the isotopic composition of the DIC initially evolved under completely open-system conditions and subsequently evolved under closed-system conditions (approach of Han & Plummer, 2013).

Less deep infiltrated mineralized waters further to the east in the Schwarzwald (Bad Teinach, Bad Liebenzell) are characterized by $d^{13}C_{CO2}$-values from − 9.9 to − 21.3 ‰ and indicate a significant contribution of organically derived carbon (Griesshaber et al., 1992) from root respiration of C3 plants (trees). Those mineralized waters represent the first stage in fluid evolution of Baden-Baden thermal water.

5 Discussion

Summarizing field, tunnel, and borehole geological data from the Oos basin we interpret the metamorphic schists as former roof rocks of the granites. Post-emplacement ductile and brittle deformation modified original geometries. Depth extent of the metamorphic schists is essentially unknown, but—as roof pendants—are limited at depth by granites. Hydrochemical and isotopic investigations of the thermal water in Florentinerquelle II indicate these rocks are not expected to extend as deep as shown in Fig. 14a. Otherwise, the thermal water would show a different hydrochemical and isotopic signature (as outlined above).

5.1 Geological setting of the geothermal fluids

NNW-striking fractures are expected to outline highest dilation tendencies and N-S-striking faults have the highest slip tendencies for sinistral lateral shear reactivation. The (N)NE-striking Main thermal-fault and the ENE-striking Rotenbach fault have rather low potentials for reactivation. Faults, subparallel to the Main thermal fault, were exposed by various constructional work in the shallow subsurface in the city area (Trinkhalle-Kurhaus, Michaels-Tunnel) provide evidence for the presence of thermal waters in the crystalline basement rocks there.

Thermal water inflow in the two boreholes Florentinerquelle I and II occurs along fractures of the fractured Friesenberg granite near the fault but not within the about 16–25 m thick Friesenberg-fault zone itself. In the much deeper well Florentinerquelle II additional inflow is documented from fractures in the metamorphic schists (Fig. 14a).

All thermal waters of Baden-Baden are welling up from fractures and small faults within the Friesenberg granite north of the Friesenberg reverse fault, from fractures within the metamorphic schists—between Friesenberg- and Main thermal fault—(thermal wells) and SE of the Main thermal fault from fractures and small faults within the Upper Carboniferous sediments (Fig. 14a), characterized by normal faulting structures (thermal springs). As the Friesenberg fault is not favorably oriented in the stress field we presume that the hanging wall granites are relatively impermeable and deep thermal water is forced to flow upwards in the fractured footwall of the NW-dipping Friesenberg fault. The Main thermal fault and Rotenbach fault, intersect each other at depth (Fig. 14a, b), likely generating a fractured basement in the footwall of the Friesenberg fault. Trend and plunge of the intersection line of both faults strongly depend on the strike and dip of the intersecting faults and can vary from steeply SE to moderately ENE plunge (Fig. 14b). Particularly, we consider steep SE plunging intersection lines as potential fluid conduits from a deep

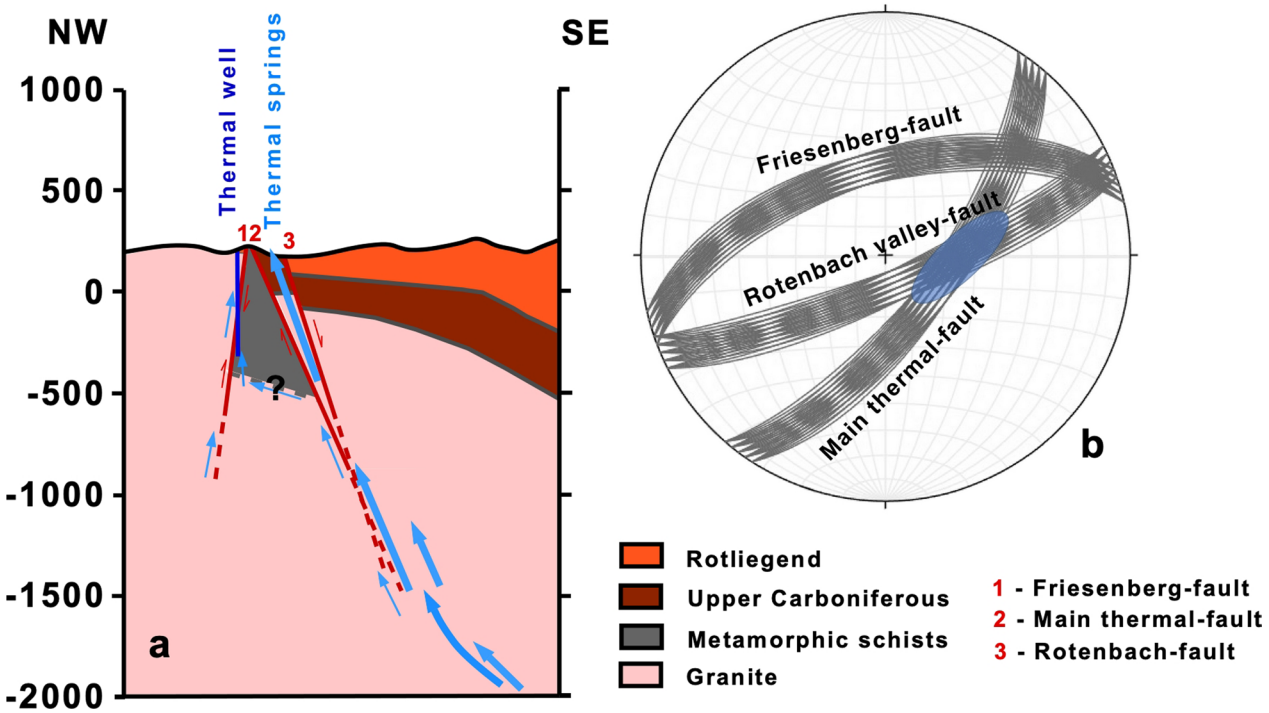

Fig. 14 Schematic cross section through the investigation area showing the location of the thermal well (Florentinerquelle II) and the thermal springs (**a**). The light blue arrows show the flow paths of upwelling thermal water. Depth position of the metamorphic schists ('old schists' in older literature) is the depth of well Florentinerquelle II (min.) and the fluid composition (max.). **b** Trend and plunge of possible intersection lines (blue area) of the Rotenbach fault and Main thermal fault is possible from ENE to SE (blue area), assuming ± 5° variance of strike and dip of the faults. Values are taken from Maus and Sauer (1972) for the Rotenbach fault (157 ± 5/80 ± 5), the Main thermal fault (127 ± 5/70 ± 5), and the Friesenberg fault (343 ± 5/60 ± 5). For reasons of depiction only 29 of 120 possible combinations of great circles are displayed for each fault

reservoir to the surface. The cumulative flow rate of 9 L s^{-1} rather indicates fluid flow in a fracture network than fluid transport in a major, favorably oriented single fault. In principle, similar geometries are expected for the Trinkhallen fault and the SE-dipping Michaels-Tunnel fault, but there only little discharge of thermal fluids in the order of several mL s^{-1} was observed.

5.2 Hydrochemical properties and evolution of the thermal waters

The water type of all thermal waters of Baden-Baden (thermal springs and thermal wells) is identical (Fig. 5B) and even the variance of the trace element concentrations and of the saturation states of the thermal waters with respect to selected minerals is very small (Figs. 9, 11), despite the thermal waters flow out from different geological units (i.e. Upper Carboniferous sediments, granites, metamorphic schists). Thus, we conclude that the thermal waters developed in the same geological reservoir. The thermal waters have a typical crystalline basement signature of deep fluids with Na and Cl as main components (e.g. Frape & Fritz, 1987; Michard, 1990; Edmunds & Savage, 1991; Pauwels et al., 1993), i.e. of deep waters residing in granites and granitic gneisses (Stober & Bucher, 2010).

Generally, TDS is increasing with depth, caused by alteration processes, whereas the sources of solutes can be identified as follows: Albite as main source for Na, biotite as source for K, Mg, and Fe, K-feldspar for K, and sulfide, like pyrite or pyrrhotite, as main source for sulfate (SO_4). Chloride originates from biotite and from fluid inclusions, which is also a minor source of additional Na. Finally, Ca and carbonate formed from plagioclase, from dissolution of secondary and fissure calcite, and from CO_2 in the recharge water (Bucher & Stober, 2010). Acidity produced by sulfide oxidation is consumed by carbonate dissolution. Calcite and related carbonates may be present as secondary alteration minerals in granites and as coatings on fractures (White et al., 2005, Walenta, 1992). The Na/Ca relationship of the thermal waters can be deduced to alteration of plagioclase under enhanced temperatures (Fig. 8).

However, TDS additionally increases passively by hydration reactions at depth, i.e. by H_2O consuming chemical reactions binding free H_2O into the structure of a hydrate mineral (e.g. zeolites like stilbite and

laumontite), not affecting pH (Stober & Bucher, 2004). In contrast to most other ions, lithium (Li) and chloride (Cl) should remain preferentially in the solution when released from minerals (phyllosilicates for Li), including fluid inclusions in quartz, because of alteration processes and thus will lead to an 'accumulation' of both elements in natural deep fluids with long residence time. The ratio of Cl- and Li concentrations of the thermal waters correspond to those of deep thermal waters in the crystalline basement, Permotriassic siliciclastic reservoir rocks and Schwarzwald (Drüppel et al., 2020) and to the thermal spring waters of Da Qaidam, China, which also evolved in granitic rocks (Stober et al., 2016, 2023).

The Cl/Br ratio (mass ratio) of the thermal waters (springs, thermal wells) varies between Cl/Br = 274 and 478 with an arithmetic mean of Cl/Br = 385 (δ = 57). Thus, in most cases it is slightly higher than the signature of modern seawater (Cl/Br = 288) and higher than Cl/Br ratios of water normally found in crystalline basement rocks. Cl/Br ratios reported from fractured granites are typically 50–100 (Frape & Fritz, 1987; Gascoyne et al., 1987; Savoye et al., 1998; Davis et al., 2001; Stober & Bucher, 2005). Shallow groundwater is characterized by low Cl/Br ratios of 80–100 (Freeman, 2007) and may be influenced by Cl/Br of atmospheric input. The Cl/Br ratio of water derived from dissolved halite deposits on the other hand is on the order of some 1000 s (Davis et al., 1998; Stober & Bucher, 1999a). The mean value of the Na/Cl ratios (molar ratio) of all thermal waters is Na/Cl = 0.90 (δ = 0.08), differing from unity (halite), and is higher than in modern seawater (Na/Cl = 0.86). Thus, the origin of Cl in the thermal waters cannot be derived from halite dissolution from previously overlaying halite strata. Also, the Cl/Br ratio might not be affected by former overlaying Triassic evaporites (Bons et al., 2014), since the estimated age of the residence time of the thermal waters is much shorter (chap. 4.4). However, the slightly enhanced Cl/Br ratio of the thermal waters with respect to fluids very often found in crystalline basement rocks might be a result of solution of small amounts of halite, present on mineral grain surfaces and/or of crushed fluid inclusions during alteration processes (Trommsdorff et al., 1985, Althaus & Bauer, 1987, Markl & Bucher, 1998, Stober & Bucher, 1999a). Enhanced Cl/Br ratios in fluid inclusions of quartz in granites are also documented from other sites (e.g. Yardley et al., 1992, Banks et al., 2000).

Summing up the hydrochemical data showed that the thermal waters of Baden-Baden evolved most probably from meteoric waters infiltrated in granitic rocks. Thermal springs often originate from precipitation in high altitudes of the mountains lying behind the thermal springs and are therefore of meteoric origin (e.g. Stober & Bucher, 2014; Stober et al., 2016). However, for the occurrence of thermal springs of Baden-Baden both, a hydraulic barrier (core of fault) and zones with enhanced permeability (intersection line of damage zones of two faults, Fig. 14a, b) are essential, and necessary.

5.3 Estimation of reservoir temperature

Differences between outflow temperatures of up to 69 °C and calculated reservoir temperatures result i.a. from the observed low- to moderate flow rates of the upwelling thermal waters. The pH of the outflow implies that dissolved SiO_2 is predominantly present as uncharged neutral complex. The estimated reservoir temperature by using quartz-geothermometry is c. 147 °C (Table 3 ESM) and reflects a minimum value, since springs are open systems allowing shallower (colder) waters with less SiO_2-content mix with the hot waters upwelling from greater depth. Additionally, precipitation of quartz in the deepest and hottest portion of the upflow segment could occur leading to a reduction SiO_2 concentration in the spring waters.

Generally, the Na/K thermometer is an excellent and robust tool for deriving T-estimates from hot water residing in granitic reservoirs (e.g. Michard, 1990; Stober & Bucher, 2021). Because it is based on a cation ratio dilution of high-TDS water with near surface water during upwelling does usually not alter the Na/K ratio of the fluid, like the SiO_2-geothermometer. The Na/K ratio of the thermal waters are dictated by the presence of two primary feldspars (K-feldspar, plagioclase). Also, the cooled fluid emerging at springs is not likely precipitating K- or Na-bearing alteration minerals. Na/K-geothermometry leaded to an estimated reservoir temperature of c. 210 °C (Table 3 ESM) by taking into account the actual composition of the involved feldspars (Stober & Bucher, 2021). Ignoring the mineralogical composition of the two feldspars would lead to higher temperature estimates. The major uncertainty related to the Na–K exchange equilibrium between the involved feldspars is the actual alteration assemblage and 'impurity' of feldspars present in the reservoir rocks. Besides, we do not have much data of the feldspars' composition, which are slightly scattering in nature (Table 4 ESM). Additionally, clay minerals could participate in the reaction and sometimes Na/K geothermometers overestimate reservoir temperatures (Stober & Bucher, 2021). Another possible reason for the calculated higher Na/K reservoir temperature—than oxygen isotope geothermometer (Table 5 ESM)—could be that sodium-dependent cation geothermometers frequently appear to overestimate reservoir temperatures, which may be caused by precipitation of albite at depth (Fowler et al., 2013).

The content of Mg and K in deep geothermal fluid is controlled by fluid interaction with mineral phases such as muscovite, chlorite, and K-feldspar (Eq. 4). Temperatures derived from the Mg/K geothermometer are subject to many concerns. Sources of error include e.g. unknown mineral compositions, inadequate activity models (particularly problematic for chlorite) and more. Another important source of error is probably the low concentration of dissolved Mg in geothermal fluids (Stober et al., 2022) and/or the possible uptake of Mg from near surface water. The various problems related to the Mg–K thermometer have been discussed in Stober and Bucher (2021). However, the application of different Mg/K geothermometers (e.g. Stober & Bucher 2021) failed and leaded to implausible low temperature estimates, probably because equilibration between the involved minerals (muscovite, chlorite) and the fluid was not yet achieved, because we did not know the mineralogical composition of the involved minerals (deviation from the mineral endmember composition especially of chlorite and muscovite), and because small errors in the determination of the Mg content or admixture of shallow groundwater leads to huge discrepancies in the Mg/K ratio.

The Giggenbach-diagram is based on the respective endmember compositions of the minerals considered in the two Eqs. 1 and 4. However, 'impure' minerals are normally present, which is why for the K-Na exchange the use of Eq. 3 instead of Eq. 2 is preferable for estimating the reservoir temperature. An equivalent equation for the Mg–K exchange (Eq. 4) is given in Stober et al. (2022). However, this requires appropriate mineral analyses. Thus, the temperature estimates in the Giggenbach (1988) triangle, based on endmember-composition of the minerals involved in the Mg–K exchange, are implausible showing a variance between 110–140 °C (Fig. 12), far below the minimum reservoir temperature. The consequence of non-equilibrium Mg–K distribution is that the waters form a linear array given by the K-Na exchange reaction involving K-feldspar and albite (Fig. 12).

Reservoir temperature estimates using different Na/Li geothermometers (e.g. Kharaka et al., 1982; Fouliac & Michard, 1981; Verma & Santoyo, 1997) leaded to implausible high temperatures. Generally, all Na/Li geothermometers are based on empirical equations, e.g. regression functions for measured data (Na/Li and temperature) and not on laws of chemistry and thermodynamics (Verma, 2015), as the other geothermometers used within this paper. Thus, several Na/Li geothermometers exist for different boundary conditions such as fluid salinity, chemical composition of the fluid, origin and nature of the rock, involvement of seawater and others (Sanjuan et al., 2016, 2021; Drüppel et al., 2020).

There are many more cation ratio geothermometers in the international literature (e.g. Michard, 1990), but it would go beyond the scope of this paper to use even more.

The measured oxygen isotope composition of dissolved sulphate (SO_4) and water (H_2O) allowed to calculate an independent reservoir temperature (Table 5 ESM). The expected reservoir temperature is above 200 °C as deduced from solute Na/K geothermometers (Table 3 ESM, Fig. 12) which provides an indication for a comparably rapid equilibration. This assumption is in line with the missing difference of the calculated reservoir temperature between the sulfate-water and bisulfate (HSO_4^-)-water geothermometer which should occur in case of low temperatures < 150 °C (Boschetti, 2013). Minimum reservoir temperature is c. 147 °C (Table 3 ESM). Therefore, we can exclude the empirical and theoretical SO_4-H_2O geothermometers of Halas and Pluta (2000) and Zeebe (2010), respectively which are valid in the temperature range 0–150 °C (Table 5 ESM). We also exclude the values obtained by the $CaSO_4$-H_2O (combined Chiba et al., 1981 and Zheng, 1999) and $BaSO_4$-H_2O (Sakai, 1977, Kusakabe & Robinson, 1977) geothermometers because the fluid is undersaturated with respect to anhydrite and only plus-minus saturated with respect to barite (Chap. 4.3.3; Fig. 11). None of the two minerals are supersaturated. The remaining reliable reservoir temperature calculated with the SO_4-H_2O geothermometers applicable in the 100–350 °C temperature range is between 170 and 180 °C. This independent isotope geothermometer provides almost identical temperatures for the springs in the galleries Kirchenstollen including Rosenstollen and the springs in distant gallery Friedrichstollen, which indicates a common reservoir and fluid evolution of the Baden-Baden thermal springs.

However, the oxygen isotopes of SO_4 and H_2O led to an estimation of reservoir temperature of c. 176 °C, which is the most trustful and reasonable value of the reservoir temperature (Lloyed, 1968; McKenzie & Trusdell, 1977)). Assuming an undisturbed temperature gradient of about gradT = 30 K km^{-1}, outside the temperature anomaly of Baden-Baden, and a mean surface temperature of 10 °C, the calculated reservoir temperatures correspond to a reservoir depth of around 5.5 km.

5.4 Results of isotope data regarding evolution and origin of the thermal waters

The sulfur and oxygen isotope composition of the dissolved sulfate point to an oxidation of sulfides in the crystalline basement (Boschetti et al., 2011). A contribution of strontium from modern (Sr = 7 mg/l; $^{87}Sr/^{86}Sr = 0.7092$) or fossil seawater with lower $^{87}Sr/^{86}Sr$ ratios can be excluded (Fig. 13A) (Peuker-Ehrenbrink &

Fiske, 2019; Veizer, 1989; Veizer et al., 1999; Mizutani & Rafter, 1969). The same holds true for lithium based on the differing lithium isotope composition of Baden-Baden fluid (δ^7Li: 1.7 ‰; Sanjuan et al., 2016) compared to the modern seawater value of 31 ‰ (e.g. Misra & Fröhlich, 2012). Hydrogen versus oxygen isotope composition indicates that the Baden-Baden fluid consists of meteoric water without any seawater component (Fig. 13B). The missing positive oxygen isotope shift suggests the absence of high-temperature alteration (> 230 °C) along the flow path in the crystalline basement (compare strontium isotope evidence above) and can be explained by low water–rock ratio along the fluid pathway in the granitic basement (Gottardi et al., 2024). The crustal helium isotope composition indicates a flow path of infiltrating rainwater through the crystalline basement (Fig. 13F) where the initial atmospheric composition is overwhelmed with crustal helium (^{4}He) because of the decay of uranium and thorium during its residence time in the subsurface.

The oxygen isotopes indicate a mean elevation of 884 ± 35 m a.s.l. of the recharge area (Fig. 13D), which is reached in the region of the 'Badener Höhe', a summit SSE of Baden-Baden (Fig. 1). Noble gases of Baden-Baden thermal fluids (Kr and Xe) show an infiltration temperature in the recharge area of 5–6 °C, which are in-line with recent yearly mean temperatures in the 900 m elevation range, i.e. the results fit to the calculated recharge elevation. Recalculated ^{14}C activity and DIC concentration indicate a mean residence time ('age') of the thermal waters of 10,800 years. The water isotope composition (mean value: $\delta^{18}O = -9.77$ ‰; $dD = -67.76$ ‰) also indicates groundwater recharge during relatively warm climate conditions in the Holocene.

5.5 Deep circulation system

The results from isotope data evaluation are in line with the investigations on water chemistry. The thermal waters cannot be derived from seawater, but from meteoric waters, infiltrating with a temperature of 5–6 °C in c. 900 m NN (Badener Höhe) in granitic rocks. Groundwater recharge occurred during warm climate conditions in the Holocene, which fits to the residence time of 10,800 years in the subsurface and to numerically modelled circulation duration of about 11,000 years (Giersch 2006). Meteoric water interacts in the deep subsurface with granitic rocks, evolving its typical crystalline basement water signature. Depth of the circulation path is about 5500 m below surface, taking into account an estimated reservoir temperature of 176 °C and an assumed undisturbed geothermal gradient of c. 30 K km^{-1}. Generally, the driving force of the deep circulation is the hydraulic gradient between mountains and valleys. During infiltration (descending path) the meteoric water has a low temperature and low TDS. Infiltration into the deeper subsurface is relatively slowly caused by the low to moderate natural permeability of the granitic rocks. Mineralization of the descending water increases because of alteration of the granitic rocks and waters acquire a 'granitic signature'. New equilibria between water and the surrounding rock (minerals) adjust in accordance with increasing pressure (p) and temperature (T). Ascent of the deep thermal waters occurs—in contrast to descent—relatively fast, else temperature of the thermal springs would be much lesser. Thus, the permeability of the ascent path must be relatively high. Most plausible ascent paths are the damage zones of the deep reaching faults (Rotenbach fault, Main thermal fault) and especially the intersection lines of these structures (Fig. 14a, b). As can be seen in Fig. 14a, the flow paths in the subsurface to the Florentinerquellen I and II are somewhat longer than to the thermal springs, which is also supported by higher He concentrations (Tab. 8 ESM).

During upwelling p/T-conditions are changing to lower values. Thus, saturation states of the hot TDS-rich water with respect to selected minerals changes and some minerals will precipitate, e.g. barite, calcite and probably albite, the latter possibly changing the Na/K ratio and thus leading to higher estimated reservoir temperatures using Na/K geothermometers. Further consequences of supersaturation are continuous clogging of the ascending flow path over time, leading to a dynamic thermal water system. Thus, continuously flowing thermal springs require tectonically active areas (e.g. occurrence of earthquakes) to re-activate flow paths. This is a continuous process (Sanjuan et al., 2016, 2021).

6 Conclusion

All thermal waters of Baden-Baden (thermal springs and thermal wells) evolved from meteoric waters in granitic rocks, independent of the different geological units (Upper Carboniferous sediments, granite, metamorphic schists) from where they are emerging. Hydrochemistry of thermal waters have a typical deep crystalline basement signature, dominated by Na and Cl. The Na/Ca relationship of the thermal waters results from alteration of plagioclase under enhanced temperatures. Li and B fits other crystalline basement correlations. Sulfur- and oxygen isotopes indicate that SO_4 in thermal waters originates from oxidation of sulfides in granitic rocks. Crustal helium isotope composition indicates a flow path of meteoric water through crystalline basement.

Thermal water is of meteoric origin with infiltration temperature of 5–6 °C and an elevation of the recharge area of c. 900 m asl. Thermal waters evolved within the

granitic rocks during a circulation duration of about 10,800 years. Geothermometry indicates a reservoir temperature for the thermal waters of > 147 °C (SiO_2 geothermometers), around 210 °C (Na/K-geothermometers), and 176 °C (Oxygen isotopes of SO_4 and H_2O), whereas the latter seems to be the most reliable value.

Metamorphic schists are former roof rocks of the granites with limited depth and therefore do not influence hydrochemistry and isotopy. Same is true for Upper Carboniferous sediments. The Rotliegend sediments are more or less hydraulically tight, acting rather as a barrier.

Though stress data from the Schwarzwald are limited and inferred from only few shallow boreholes (TVD < 500 m), they indicate a strike-slip regime and a general (N)NW-(S)SE trending S_{Hmax}, which may be the preferred direction of fluid transport in the crystalline basement of the Schwarzwald whereas the NE-trending structures in Baden-Baden rather act as hydraulic barriers forcing the thermal fluids to emerge to the surface. Upwelling of the thermal water occurs along damage zones of two deep reaching faults in granitic rocks. While none of these faults is favorably oriented in the stress field, the steep SE-plunging intersection of the two fault damage zones seems to be relevant for the upward thermal water transport from the granitic reservoir, penetrating the overlaying thin sediments (Upper Carboniferous sediments, metamorphic schists).

Thus, the hydrochemical, isotopic, and structural geological investigations carried out on the thermal waters in the Baden-Baden area yielded results on the fluid origin of the thermal waters, on the location of the recharge area, and on genesis and residence time of the thermal waters in the deep granitic subsurface. Based on these results, it seems very likely to obtain with comparable investigations at geothermal sites in granitic rocks a quantitative understanding of available fluid quantities, fluid development, as well as circulation, transport and storage of fluids in geothermal reservoirs, important information for a sustainable and responsible use of energy and raw materials from deep geothermal fluids. In order to evaluate the groundwater age, the origin and genesis, as well as the migration paths of deep fluids, the investigation of noble gases or noble gas isotopes and their ratios plays a particularly important role.

Supplementary Information

The online version contains supplementary material available at https://doi.org/10.1186/s00015-025-00480-z.

Supplementary Material 1.

Supplementary Material 2.

Supplementary Material 3.

Supplementary Material 4.

Supplementary Material 5.

Supplementary Material 6.

Supplementary Material 7.

Supplementary Material 8.

Acknowledgements
We would like to thank the staff of the thermal spa Baden-Baden and Tiefbauamt Baden-Baden for supporting us with unpublished reports, Kirsten Drüppel for providing geochemical analyses of feldspars from the Nordschwarzwald, Ezgi Keskin for support in sampling and support of analytical work in the laboratory, and Harald Strauß for provision of analytical facilities in Münster University. We also would like to thank two anonymous reviewers and the editor for their help to improve the paper.

Author contributions
IS carried out fieldwork, analyzed and interpreted the hydrochemical data, drafted figures, tables, and the manuscript. JG carried out fieldwork, analyzed geological data, and drafted figures. MK carried out fieldwork, analyzed and interpreted isotopic data, drafted figures and tables. All authors contributed to the final text of the manuscript. All authors read and approved the final submission.

Funding
Open Access funding enabled and organized by Projekt DEAL.

Availability of data and materials
No datasets were generated or analysed during the current study.

Declarations

Competing interests
The authors declare no competing interests.

Received: 25 November 2024 Accepted: 28 March 2025
Published online: 09 May 2025

References

Agemar, T., Hese, F., Moeck, I., & Stober, I. (2017). Kriterienkatalog für die Erfassung tiefreichender Störungen und ihrer geothermischen Nutzbarkeit in Deutschland. *Zeitschrift der Deutschen Gesellschaft für Geowissenschaften., 168*(2), 285–300.

Althaus, E. & Bauer, F. (1987). Berichte des Arbeitskreises Geochemie. In: Althaus, E. et al., eds. Endbericht über erweiterte Zirkulation wässriger Fluide im Hot Dry Rock System (Gneisgebirge) der Bohrung Urach 3, 176–212, (unpublished).

Ambs S. (2002). Geologische und hydrogeologische Untersuchung in Neusatz (Baden) und Umgebung. Unpublished diploma thesis at University Karlsruhe, 121 pages.

Aquilina, L., Pauwels, H., Genter, A., & Fouillac, C. (1997). Water-rock interaction processes in the Triassic sandstone and the granitic basement of the Rhine Graben: geochemical investigation of a geothermal reservoir. *Geochimica et Cosmochimica Acta, 61*, 4281–4295.

Arnórsson, S. (1983). Chemical equilibria in Iceland geothermal systems. Implications for chemical geothermometry investigations. *Geothermics, 24*, 603–629.

Banks, D. A., Green, R., Cliff, R. A., & Yardley, B. W. D. (2000). Chlorine isotopes in fluid inclusions: Determination of the origins of salinity in magmatic fluids. *Geochimica et Cosmochimica Acta, 64*(10), 1785–1789.

Basler, R. (1989b). Michaelstunnel Baden-Baden. Geologische / Hydrogeologische Dokumentation: Hydrogeologie. Abschlussbericht, 200 pp, (unpublished).

Basler, R. (1989a). Michaelstunnel Baden-Baden. Geologische / Hydrogeologische Dokumentation: Geologie. Abschlussbericht, 177 pp, (unpublished).

Bender, K. (1995). Herkunft und Entstehung der Mineral- und Thermalwässer im nördlichen Schwarzwald. *Heidelberger Geowissenschaftliche Abhandlungen*, 85, 145 S. Heidelberg.
Beyer, A. (1788). Geognostische und bergmännische Bemerkungen auf einer im Jahre 1788 gemachten Reise in die Hochfürstl. Markgräfl. Badischen Lande. *Beiträge zur Bergbaukunde I*, GLA, Karlsruhe.
Bilharz, A. (1934). Geologische Spezialkarte von Baden - Erläuterungen zu Blatt Baden (Nr. 67). *Badische Geologische Landesanstalt*, 144 S., Herder Verlag, Freiburg.
Blatt, H., & Tracy, R.J. (1996). Petrology; igneous, sedimentary, and metamorphic. W. H. Freeman, (2nd ed.). ISBN 0-7167-2438-3.
Bons, P. D., Fusswinkel, T., Gomez-Rivas, E., Markl, G., Wagner, T., & Walter, B. (2014). Fluid mixing from below in unconformity-related hydrothermal ore deposits. *Geology, 42*, 1035–1038.
Boschetti, T. (2013). Oxygen isotope equilibrium in sulfate–water systems: A revision of geothermometric applications in low-enthalpy systems. *Journal of Geochemical Exploration, 124*, 92–100.
Boschetti, T., Cortecci, G., Toscani, L., & Iacumin, P. (2011). Sulfur and oxygen isotope compositions of Upper Triassic sulfates from Northern Apennines (Italy): Palaeogeographic and hydrogeochemical implications. *Geologica Acta, 9*, 129–147.
Bozorg-Mehri, K. (1989). Der Michaelstunnel - Geologische Verhältnisse, Geomechanisches Gebirgsverhalten, Untersuchungen zur Bohrbarkeit. 207 S., Dipl.-Arb. TU München (unveröff.).
Bucher, K. (2023). *Petrogenesis of metamorphic rocks* (9th ed.). Springer publisher.
Bucher, K. spsampsps Stober, I. (2000). The composition of groundwater in the continental crystalline crust. In: Stober, I. spsampsps Bucher, K. (eds.) *Hydrogeology in crystalline rocks*. KLUWER academic Publishers, p. 141–176.
Bucher, K., & Stober, I. (2010). Fluids in the upper continental crust. *Geofluids, 10*, 241–253. https://doi.org/10.1111/j.1468-8123.2010.00279.x
Bucher, K., Zhang, L., & Stober, I. (2009a). A hot spring in granite of the Western Tianshan, China. *Applied Geochemistry, 24*, 402–410. https://doi.org/10.1016/j.apgeochem.2008.12.021
Bucher, K., Zhu, Y., & Stober, I. (2009b). Groundwater in fractured crystalline rocks, the Clara mine, Black Forest (Germany). *International Journal of Earth Science (Geol. Rundschau), 98*, 1727–1739. https://doi.org/10.1007/s00531-008-0328-x
Caine, J. S., Evans, J. P., & Forster, C. B. (1996). Fault zone architecture and permeability structure. *Geology, 24*(11), 1025–1028.
Can, I. (2002). A new improved Na/K geothermometer by artificial neutral networks. *Geothermics, 31*(6), 751–760. https://doi.org/10.1016/S0375-6505(02)00044-5
Carasana. (2004). Quellbuch. Aufzeichnungen seit 1894 über halbjährliche Kontrollmessungen von Temperatur und Schüttung der Thermalquellen und der Pflutterlochbohrungen. Friedrichsbad Baden-Baden, CARASANA Bäderbetriebe GmbH, Baden-Baden.
Carlé, W. (1975). *Die Mineral- und Thermalwässer von Mitteleuropa*. Verlagsgesellschaft, Stuttgart.
Cerling, T. E., Harris, J. M., MacFadden, B. J., Leakey, M. G., Quade, J., Eisenmann, V., & Ehleringer, J. R. (1997). Global vegetation change through the Miocene/Pliocene boundary. *Nature, 389*, 153–158. https://doi.org/10.1038/38229
Chiba, H., Kusakabe, M., Hirano, S., Matsuo, S., & Somiya, S. (1981). Oxygen isotope fraction factors between anhydrite and water from 100°C and 550°C. *Earth and Planetary Science Letters, 53*, 55–62.
Choi, J. H., Edwards, P., Ko, K., & Kim, Y. S. (2016). Definition and classification of fault damage zones: A review and a new methodological approach. *Earth-Science Reviews, 152*, 70–87.
Davis, S. N., DeWayne, C. L., Zreda, M., & Moysey, S. (2001). Chlorine-36, bromide, and the origin of spring water. *Chemical Geology, 179*, 3–16.
Davis, S. N., Whittemore, D. O., & Fabryka-Martin, J. (1998). Uses of chloride/bromide ratios in studies of potable water. *Ground Water, 36*, 338–350.
Dezayes, C., & Lerouge, C. (2019). Reconstructing paleofluid circulation at the hercynian basement/ mesozoic sedimentary cover interface in the Upper Rhine Graben. *Geofluids*. https://doi.org/10.1155/2019/4849860
Drüppel, K., Stober, I., Grimmer, J. C., & Mertz-Kraus, R. (2020). Experimental alteration of granitic rocks: Implications for the evolution of geothermal brines in the Upper Rhine Graben Germany. *Geothermics*. https://doi.org/10.1016/j.geothermics.2020.101903
Edmunds, W. M., & Savage, D. (1991). Geochemical characteristics of groundwater in granites and related crystalline rocks. In R. A. Downing & W. B. Wilkinson (Eds.), *Applied groundwater hydrology, a British perspective* (pp. 199–216). Clarendon Press.
Eisbacher G.H., & Fielitz W. (2010). Karlsruhe und seine Region. Sammlung Geologscher Führer, Gebrüder Bornträger Stuttgart, 103, 342 pp.
Eisele, H. (1907). Das Übergangsgebirge bei Baden-Baden, Ebersteinburg, Gaggenau und Sulzbach und seine Kontaktmetamorphose durch das Nordschwarzwälder Granitmassiv. *Zeitschrift der Deutschen Geologischen Gesellschaft, 59*, 131–214.
Faulkner, D. R., Jackson, C. A. L., Lunn, R. J., Schlische, R. W., Shipton, Z. K., Wibberley, C. A. J., & Withjack, M. O. (2010). A review of recent developments concerning the structure, mechanics and fluid flow properties of fault zones. *Journal of Structural Geology, 32*(11), 1557–1575. https://doi.org/10.1016/j.jsg.2010.06.009
Fouillac, C., & Michard, G. (1981). Sodium/lithium ratio in water applied to geothermometry of geothermal reservoir. *Geothermics, 10*, 55–74.
Fournier, R. O. (1977). Chemical geothermometers and mixing models for geothermal systems. *Geothermics, 5*, 41–50.
Fournier, R. O., & Potter, R. W., II. (1982). An equation correlating the solubility of quartz in water from 25°C to 900°C at pressures up to 10,000 bar. *Geochimica et Cosmochimica Acta, 46*, 1969–1973.
Fowler, A. P. G., Hackett, L. B., & Klein, C. W. (2013). Reformulation and performance evaluation of the sulfate-water oxygen isotope geothermometer. *GRC Transactions, 37*, 393–401.
Frape, S. K., & Fritz, P. (1987). Geochemical trends for groundwaters from the Canadian shield. In P. Fritz & S. K. Frape (Eds.), *Saline Water and Gases in Crystalline Rocks, 33* (pp. 19–38). Geological Association of Canada Special Paper.
Freeman, J. T. (2007). The use of bromide and chloride mass ratios to differentiate salt-dissolution and formation brines in shallow groundwaters of the Western Canadian Sedimentary Basin. *Hydrogeology Journal, 15*, 1377–1385.
Fröhler, M. & Lebede, S. (1987). Grundgebirge und vulkanosedimentäres Jungpaläozoikum südwestlich der Oos bei Baden-Baden. Dipl.-Arbeit, 130 S., Universität Freiburg.
Friedrichsen, H. (1981). Geothermal Systems in the Upper Rhine Graben and Northern Black Forest: A Chemical andStable Isotope Study. Development in Geotectonics. 17, 125-140,https://doi.org/10.1016/B978-0-444-41956-9.50016-2.
Gascoyne, M., Davison, C. C., Ross, J. D., & Pearson, R. (1987). Saline groundwaters and brines in plutons in the Canadian Shield. In P. Fritz & S. K. Frape (Eds.), *Saline water and gases in crystalline rocks, 33* (pp. 53–68). Geological Association of Canada Special Paper.
Giersch, C. (2006). Thermohydraulik des kristallinen Grundgebirges am Beispiel des östlichen Oberrheingrabens. Dissertation Univ. Karlsruhe.
Geyer, O.F. & Gwinner, M.P. (2011). Geologie von Baden-Württemberg. Schweizerbart Science Publishers, 627 S., ISBN 978-3-510-65267-9.
Giggenbach, W. (1988). Geothermal solute equilibria-derivation of Na-K-Mg-Ca geoindicators. *Geochimica et Cosmochimica Acta, 52*, 2749–2765.
Glodny, J., & Grauert, B. (2009). Evolution of a hydrothermal fluid-rock interaction system as recorded by Sr isotopes: A case study from the Schwarzwald, SW Germany. *Mineralogy and Petrology, 95*(3–4), 163–178. https://doi.org/10.1007/s00710-008-0034-1
Göb, S., Loges, A., Nolde, N., Bau, M., Jacob, D. E., & Markl, G. (2013). Major and trace element compositions (including REE) of mineral, thermal, mine and surface waters in SW Germany and implications for water–rock interaction. *Applied Geochemistry, 33*, 127–152. https://doi.org/10.1016/j.apgeochem.2013.02.006
Gottardi, R., Mire, C., Davis, N., & Casale, G. (2024). Effect of water-rock ratio on the stable isotope record of fluid-rock-deformation interactions in detachment shear zone. *Geochemistry, Geophysics, Geosystems*. https://doi.org/10.1029/2023GC011340
Griesshaber, E., O'Nions, R. K., & Oxburgh, E. R. (1992). Helium and carbon isotope systematics in crustal fluids from the Eifel, the Rhine Graben and Black Forest F.R.G. *Chemical Geology, 99*(4), 213–235.
Grimm, B., Franz, M., Kilger, B.-M., Lorenz, G., & Schmidt-Witte, H. (2005). Die Thermalwassererschließung im Muschelkalk von Tuttlingen. *Berichte der Naturforschenden Gesellschaft Zu Freiburg i Br, 95*(1), 189–212.
Grimmer, J. C., Ritter, J., Eisbacher, G. H., & Fielitz, W. (2017). The late Variscan control on the location and asymmetry of the Upper Rhine Graben.

International Journal of Earth Sciences, 106(3), 827–853. https://doi.org/10.1007/s00531-016-1336-x

Halas, S., & Pluta, I. (2000). Empirical calibration of isotope thermometer $\delta^{18}O(SO_4^{2-})$–$\delta^{18}O(H_2O)$ for low temperature brines. *V Isotope Workshop, European Society for Isotope Research*, Kraków, Poland, 68–71.

Han, L. F., & Plummer, L. N. (2013). Revision of Fontes & Garnier's model for the initial 14C content of dissolved inorganic carbon used in groundwater dating. *Chemical Geology, 351*, 105–114.

Hauser-Fuhlberg, M., Rahn, W., Rothengatter, P., Bechler, K., Mainka, U. (2012). Pumpspeicherwerk Forbach. Geotechnisches und hydrogeologisches Gutachten.

Heidbach, O., Rajabi, M., Reiter, K., Ziegler, M. and the WSM Team (2016). World Stress Map Database Release 2016, GFZ Data Services, https://doi.org/10.5880/WSM.2016.001

Holland, T. J. B., & Powell, R. (2011). An improved and extended internally consistent thermodynamic dataset for phases of petrological interest, involving a new equation of state for solids. *Journal of Metamorphic Geology, 29*, 333–383.

Johnson, J. W., Oelkers, E. H., & Helgeson, H. S. (1992). SUPCRT92: A software package for calculating the standard molal thermodynamic properties of minerals, gases, aqueous species, and reactions from 1 to 5000 bar and 0 to 1000°C. *Computers and Geosciences, 18*, 899–947.

Käß, W. (1995). 2. Thermen. In: LADBW (1995), 26–37.

Käß, W. & Käss H. (2008). Deutsches Bäderbuch. 2nd ed., Schweizerbart'sche Verlagsbuchhandlung, 1232 p., Stuttgart.

Kharaka, Y. K., Lico, M. S., & Lax, L. M. (1982). Chemical geothermometers applied to formation waters, Gulf of Mexico and California basins. *Bulletin of the American Association of Petroleum Geologists., 66*, 588.

Kiderlen, H. (1953). Zur Geologie der Schwarzwaldthermen. *Neues Jahrbuch für Geologie und Paläontologie, 96*, 496–506.

Kirchheimer, F. (1959). Über radioaktive und uranhaltige Thermalsedimente, insbesondere von Baden-Baden. *Abh. geol. Landesamt Bad.-Württ.*, 3, 1–67, Freiburg.

Krohe, A., & Eisbacher, G. H. (1988). Oblique crustal detachment in the Variscan Schwarzwald, southwestern Germany. *Geologische Rundschau, 77*, 25–43.

Kusakabe, M., & Robinson, B. W. (1977). Oxygen and sulfur isotope equilibria in the system from 110 to 350 °C and applications. *Geochimica et Cosmochimica Acta, 41*, 1033–1040.

Lawrence Livermore National Laboratory. (2020). Lawrence Livermore National Laboratory (LLNL) Open Data Initiative. UC San Diego Library Digital Collections. https://doi.org/10.6075/J0HD7T2Q

Lloyd, R. M. (1968). Oxygen isotope behavior in the sulfate-water system. *Journal of Geophysical Research, 73*(18), 6099–6110.

Löffler, M. (1988). Ein Beitrag zur Strukturgeologie des Battertkristallins zwischen Ebersteinburg und Baden-Baden (Zone von Baden-Baden, Nordschwarzwald). Dipl.-Arb., Univ. Karlsruhe, 115 p. (unpublished).

Markl, G., & Bucher, K. (1998). Metamorphic salt in granulites: Implications for the presence and composition of fluids in the lower crust. *Nature, 391*, 781–783.

Maus, H. & Sauer, K. (1972). Die Thermalwasserbohrungen im Gewann Pflutterloch auf Gemarkung Baden-Baden - Balneo- und regionalgeologische Ergebnisse. *Mitt. Bad. Landesver. Naturkunde u. Naturschutz*, 10/3, 469–480, Freiburg.

McKenzie, W. F., & Truesdell, A. H. (1977). Geothermal reservoir temperatures estimated from oxygen isotope compositions of dissolved sulfate and water from hot springs and shallow drillholes. *Geothermics, 5*, 51–62.

Meixner, J., Grimmer, J. C., Becker, A., Schill, E., & Kohl, T. (2018). Comparison of different digital elevation models and satellite imagery for lineament analysis: Implications for identification and spatial arrangement of fault zones in crystalline basement rocks of the southern Black Forest (Germany). *Journal of Structural Geology, 108*, 256–268.

Metz, R. (1977). Mineralogisch-landeskundliche Wanderungen im Nordschwarzwald. 2. Aufl., 632 S., Moritz Schauenburg Verlag, Lahr, Germany.

Michard, G. (1990). Behaviour of major elements and some trace elements (Li, Rb, Cs, Sr, Fe, Mn, W, F) in deep hot waters from granitic areas. *Chemical Geology, 89*, 117–134.

Misra, S., & Fröhlich, P. N. (2012). Lithium isotope history of Cenozoic seawater: Changes in silicate weathering and reverse weathering. *Science, 335*, 818–823.

Mitjanas, G., Walsh, J. J., Roca, E., Alías, G., Queralt, P., Ledo, J., & Pina-Varas, P. (2024). The importance of structural complexity in the localization of geothermal systems: A case study along the Vall`es-Pened`es Fault in the Catalan Coastal Ranges (NE Spain). *Geothermics*. https://doi.org/10.1016/j.geothermics.2023.102855

Mizutani, Y., & Rafter, T. A. (1969). Oxygen isotopic fractionation in the bisulphate ion-water system. *New Zealand Journal of Science, 12*(1), 54–59.

Montenari, M., & Servais, T. (2000). Early Paleozoic (Late Cambrian-Early Ordovician) acritarchs from the metasedimentary Baden-Baden–Gaggenau zone (Schwarzwald, SW Germany). *Review of Palaeobotany and Palynology, 113*(1–3), 73–85.

Müller-Hereth (1982). Geologisches Längsprofil durch den Michaelstunnel mit Ergänzungen von Löffler 1988 sowie Fröhler & Lebede 1987. Report of the engineering firm Müller-Hereth (unpublished).

Nitsch, E., & Zedler, H. (2009). Oberkarbon und Perm in Baden-Württemberg. *LGRB-Informationen, 22*, 7–102.

Orville, P. M. (1972). Plagioclase cation exchange equilibria with aqueous chloride solution: Results at 700°C and 2000 bars in the presence of quartz. *American Journal of Science, 272*, 234–272.

Parkhurst, D.L. & Appelo, C.A.J. (1999). PHREEQC (Version2)—a computer program for speciation, batch-reaction, one dimensional transport, and inverse geochemical calculations. *US Geological Survey Water-Resources Investigation Report*, 99–4259.

Pastorelli, S., Marini, L., & Hunziker, J. (2001). Chemistry, isotope values (dD, d ^{18}O, d $^{34}S_{SO4}$) and temperatures of the water inflows in two Gotthard tunnels, Swiss Alps. *Applied Geochemistry, 16*, 633–649.

Pauwels, H., Fouillac, C., & Fouillac, A. M. (1993). Chemistry and isotopes of deep geothermal saline fluids in the Upper Rhine Graben: Origin of compounds and water-rock interactions. *Geochimica et Cosmochimica Acta, 57*, 2737–2749.

Pearson, F.J. Jr. & Hanshaw, B.B. (1970). Sources of dissolved carbonate species in ground water and their effects on carbon-14 dating. *IEA*, SM-129/18, Vienna, Austria.

Peucker-Ehrenbrink, B., & Fiske, G. J. (2019). A continental perspective of the seawater $^{87}Sr/^{86}Sr$ record: A review. *Chemical Geology, 510*, 140–165.

Plenefisch, T. & Bonjer, K. (1997). The stress field in the Rhine Graben area inferred from earthquake focal mechanisms and estimation of frictional parameters. Tectonophysics, *275*, 71-97, https://doi.org/10.1016/S0040-1951(97)00016-4.

Rupf, I. & Nitsch, E. (2008). Das Geologische Landesmodell von Baden-Württemberg: Datengrundlagen, technische Umsetzung und erste geologische Ergebnisse. *LGRB-Informationen*, 21, Freiburg.

Sakai, H. (1977). Sulfate–water isotope thermometry applied to geothermal systems. *Geothermics, 5*, 67–74.

Sanjuan, B., Millot, R., Innocent, C., Dezayes, C., Scheiber, J., & Brach, M. (2016). Major geochemical characteristics of geothermal brines from the Upper Rhine Graben granitic basement with constraints on temperature and circulation. *Chemical Geology, 428*, 27–47. https://doi.org/10.1016/j.chemgeo.2016.02.021

Sanjuan, B., Négrel, G., Le Lous, M., Poulmarch, E., Gal, F., & Damy, P.-C. (2021). Main geochemical characteristics of the deep geothermal brine at Vendenheim (Alsace, France) with constraints on temperature and fluid circulation. *Proceedings World Geothermal Congress* 2020+1, 12 p., Reykjavik, Iceland.

Sanner, B. (2000). Baden-Baden, a famous thermal spa with a long history. *GHC Bulletin*, 16–22.

Sauer, K. (1966). Die Thermen von Baden-Baden und ihre erdgeschichtlichen Ursachen. In: So heilt Baden-Baden, 9–17, Uelzen.

Savoye, S., Aranyossy, J.-F., Beaucaire, C., Cathelineau, M., Louvat, D., & Michelot, J.-L. (1998). Fluid inclusions in granites and their relationships with present-day groundwater chemistry. *European Journal of Mineralogy, 10*, 1215–1226.

Schrage, C.L. (2004). Dreidimensionale thermohydraulische Modellierung der Tiefenwasserzirkulation am Westrand des Schwarzwaldes am Beispiel der Baden-Badener Thermalquellen. Diplomarbeit Universität Karlsruhe, 113 S., Karlsruhe.

Seltzer, A. M., Ng, J., Aeschbach, W., Kipfer, R., Kulongoski, J. T., Severinghaus, J. P., & Stute, M. (2021). Widespread six degrees Celsius cooling on land during the Last Glacial Maximum. *Nature, 593*, 228–232.

Sittig, E. (1965). Der geologische Bau des variszischen Sockels nordöstlich von Baden-Baden (Nordschwarzwald). *Oberrheinische Geologische Abhandlungen, 14*, 167–207.
Stober, I. (1995). Die Wasserführung des kristallinen Grundgebirges. Ferdinand Enke Verlag, 191 S., Stuttgart.
Stober, I. (1996). Geohydraulik und Hydrochemie der Thermalquellen von Bad Wildbad, Bad Liebenzell, Baden-Baden und Bad Säckingen. *DGM, 40*(2), 69–83.
Stober, I., & Bucher, I. (2010). Fluids in the upper continental crust. *Geofluids, 10*, 241–253. https://doi.org/10.1111/j.1468-8123.2010.00279.x
Stober, I., & Bucher, K. (1999a). Origin of salinity of deep groundwater in crystalline rocks. *Terra Nova, 11*, 181–185.
Stober, I., & Bucher, K. (1999b). Deep groundwater in the crystalline basement of the Black Forest region. *Applied Geochemistry, 14*, 237–254.
Stober, I. & Bucher, K. (2021). Geothermal Energy, from House Heating Applications to Electrical Power Production. 2nd edition, 390 p., Springer.
Stober, I., & Bucher, K. (2004). Fluid sinks within the Earth's crust. *Geofluids, 4*, 143–151.
Stober, I., & Bucher, K. (2005). The upper continental crust, an aquifer and its fluid: Hydraulic and chemical data from 4 km depth in fractured crystalline basement rocks at the KTB test site. *Geofluids, 5*, 8–19.
Stober, I., & Bucher, K. (2014). Hydraulic conductivity of fractured upper crust: Insights from hydraulic tests in boreholes and fluid-rock interaction in crystalline basement rocks. *Geofluids, 16*, 161–178. https://doi.org/10.1111/gfl.12104
Stober, I., Ladner, F., Hofer, M., & Bucher, K. (2022). The deep Basel-1 geothermal well: An attempt assessing the predrilling hydraulic and hydrochemical conditions in the basement of the Upper Rhine Graben. *Swiss Journal of Geosciences, 115*(3), 18. https://doi.org/10.1186/s00015-021-00403-8
Stober, I., Zhong, J., & Bucher, K. (2023). From freshwater inflows to salt lakes and salt deposits in the Qaidam Basin, W China. *Swiss Journal of Geosiences*. https://doi.org/10.1186/s00015-023-00433-4
Stober, I., Zhong, J., Zhang, L., & Bucher, K. (2016). Deep hydrothermal fluid–rock interaction: The thermal springs of Da Qaidam, China. *Geofluids, 16*, 711–728. https://doi.org/10.1111/gfl.12190
Strauss, H. (1997). The isotopic composition of sedimentary sulfur through time. *Palaeogeography, Palaeoclimatology, Palaeoecology, 132*, 97–118.
Stumm, W. & Morgan, J.J. (1975). Aquatic chemistry. 2. Aufl., 760 p., Wiley and Sons.
Thuro, K. (1998). Bohrbarkeit beim konventionellen Sprengvortrieb—Geologisch-felsmechanische Untersuchungen anhand sieben ausgewählter Tunnelprojekte. *Münchner Geol. Hefte*, B 1, 149 S., München.
Trommsdorff, A. V., Skippen, G., & Ulmer, P. (1985). Halite and Sylivite as solid inclusions in high-grade metamorphic rocks. *Contr. Miner- Petrol., 89*, 24–29.
Van Geldern, R., Baier, A., Subert H.L., Kowol, S., Balk, L., Barth, J.A.C. (2014). Hydrogen and oxygen stable isotope analyses of precipitation sampled at Erlangen (southern Germany) between 2010 and 2013. PANGAEA, *496*, 107-115,https://doi.org/10.1594/PANGAEA.833840.
Veizer, J. (1989). Strontium isotopes in seawater through time. *Annual Review of Earth and Planetary Sciences, 17*, 141–167.
Veizer, J., Ala, D., Azmy, K., Bruckschen, P., Buhl, D., Bruhn, F., Carden, G. A. F., Diener, A., Ebneth, S., Godderis, Y., Jasper, T., Korte, C., Pawellek, F., Podlaha, O. G., & Strauss, H. (1999). $^{87}Sr/^{86}Sr$, $\delta^{13}C$ and $\delta^{18}O$ evolution of Phanerozoic seawater. *Chemical Geology, 161*, 59–88.
Verma, M.P. (2015). Chemical and isotopic geothermometers to estimate geothermal reservoir temperature and vapor fraction. *Proceedings World Geothermal Congress*, Melbourne, Australia.
Verma, M.P. (2000). Revised quartz solubility temperature dependence equation along the water-vapor saturation curve. *Proceedings World Geothermal Congress*, 1927–1932, Kyushu-Tohoku, Japan.
Verma, S. P., & Santoyo, E. (1997). Improved equations for Na/K, Na/Li, and SiO_2 geothermometers by outlier detection and rejection. *Journal of Volcanology and Geothermal Research, 79*, 9–23.
von Gehlen, K., Kleinschmidt, G., Stenger, R., Wilhelm, H., & Wimmenauer, W. (1986). *Kontinentales Tiefbohrprogramm der Bundesrepublik Deutschland (KTB) – Ergebnisse der Vorerkundungsarbeiten (Lokation Schwarzwald). 2* (p. 160). KTB-Kolloquium Seeheim.
Walenta, K. (1992). Die Mineralien des Schwarzwaldes und ihre Fundstellen. Weise-Verlag, 336 S., München.
Walther, J. V., & Helgeson, H. C. (1977). Calculation of the thermodynamic properties of aqueous silica and the solubility of quartz and its polymorphs at high pressures and temperatures. *American Journal of Science., 277*, 1315–1351.
White, A. F., Schulz, M. S., Lowenstern, J. B., Vivit, D. V., & Bullen, T. D. (2005). The ubiquitous nature of accessory calcite in granitoid rocks: Implications for weathering, solute evolution, and petrogenesis. *Geochimica et Cosmochimica Acta, 69*, 1455–1571.
Wickert, F., Altherr, R., & Deutsch, M. (1990). Polyphase Variscan tectonics and metamorphism along a segment of the Saxothuringian-Moldanubian boundary: The Baden-Baden Zone, northern Schwarzwald (FRG). *Geologische Rundschau, 79*, 627–647.
Yardley, B.W.D., Banks, D.A., & Munz I.A. (1992). Halogen composition of fluid inclusions as tracers of crustal fluid behaviour. In: Kharaka & Maest (eds.), Water-rock interaction, 1137–1140.
Zeebe, R. E. (2010). A new value for the stable oxygen isotope fractionation between dissolved sulfate ion and water. *Geochimica et Cosmochimica Acta, 74*, 818–828.
Zheng, Y.-F. (1999). Oxygen isotope fractionation in carbonate and sulfate minerals. *Geochemical Journal, 33*, 109–126.
Zimmer, K., Zhang, Y., Lu, P., Chen, Y., Zhang, G., Dalkilic, M., & Zhu, Ch. (2016). SUPCRTBL: A revised and extended thermodynamic dataset and software package of SUPCRT92. *Computers and Geosciences, 90*, 97–111.
Zuther, M., & Brockamp, O. (1988). The fossil geothermal system of the Baden-Baden trough (northern Black Forest, FR Germany). *Chemical Geology, 71*(4), 337–353.

Publisher's Note